DEFORMATION STUDIES ON

ALPHA-BETA BRASS

By

Nitin Sudhakar Kulkarni

A THESIS

Submitted to
Michigan State University
in partial fulfillment of the requirements
for the degree of

MASTER OF SCIENCE

Department of Metallurgy, Mechanics and Materials Science

1984

ABSTRACT

DEFORMATION STUDIES ON ALPHA-BETA BRASS

By

Nitin Sudhakar Kulkarni

The deformation structure in polycrystalline specimens of two-phase alpha-beta brass was analyzed by Transmission Electron Microscopy, after deforming the specimens to two different strain levels (5 and 8 percents). In specimens that were deformed to 5 percent strain level, the dislocations were confined to single slip bands and no cross-slip was observed. On the other hand, specimens that were deformed to 8 percent strain level revealed complex tangled dislocations and deformation on intersecting slip planes. Burgers vector analysis of "Dislocation-Pairs", observed in the alpha phase,suggests that they may be screw dislocations that have double cross-slipped onto parallel slip planes.

The stress-strain relationships and stress-strain distributions in the two-phase alpha-beta brass were also studied by using a continuum mechanics approach with the use of Finite Element Method Analysis. This analysis was performed by using the ANSYS computer program.

ACKNOWLEDGEMENTS

I would like to take this opportunity to sincerely thank my advisor, Dr. K. N. Subramanian, but for whose guidance and encouragement this endeavour would not have ended successfully. I also take this opportunity to extend my most sincere gratitude to Dr. N. Altiero without whose advice and guidance, the Finite Element Analysis could not have been carried out. His help is greatly appreciated.

A special thanks to my colleagues, S. Shekhar and Tong C. Lee, for having helped me during the TEM investigations. This work could not have been completed without the help of all the aforementioned.

TABLE OF CONTENTS

LIST OF FIGURES

LIST OF TABLES

I. INTRODUCTION

Two-phase materials find wide ranging engineering applications. Various steels, two-phase titanium-aluminum alloys, copper-zinc alloys, copper-tin alloys and copper-aluminum alloys are some of the most widely used two-phase alloys. The mechanical properties of these two-phase materials will differ with changes in the properties of individual phases, the distribution and volume fractions of each phase. Other metallurgical factors that affect the mechanical properties of such two-phase materials are crystal structure of each phase, crystallographic orientation of the phases in relation to each other, strain-hardening in each phase, strain-rate effects and the dislocation behavior and slip in each phase.

A polycrystalline aggregate of single-phase material consists of grains which are of the same crystal structure. In such single-phase materials, different regions with different crystallographic orientations are separated by grain boundaries. In a two-phase alloy, each phase has a different chemical composition, which quite often possesses a different crystal structure. The boundary between the two phases in a two-phase material is called a phase boundary which is analogous to a grain boundary of a polycrystalline single-phase material.

In order to understand the basic mechanical behavior of a single-phase material, a single crystal or a series or parallel type bicrystal is commonly used. In a series bicrystal the grain boundary is oriented normal to the loading axis, whereas in the parallel type bicrystal, the grain boundary is oriented parallel to the loading axis. The ideal unit to study the behavior of a two-phase material is a two-phase bicrystal or a multicrystal (1,2,3). Two-phase bicrystal incorporates a single crystal of one phase joined to a single crystal of the other phase. In a multicrystal, a single crystal of one phase is joined to a few large grains of the other phase (3). A duplex crystal in which the two phases have a definite relative crystallographic orientation relationship is also of interest (3). Hingwe *et al.* (1,2,3) and Nilsen *et al.* (4,5,6) have studied the mechanical properties of bicrystals of alpha-beta brass at room temperature under uniaxial tension, at various strain-rates. Kezri-Yazdan *et al.* (7,8,9) have studied the effect of temperature on mechanical behavior of such specimens at elevated temperatures.

All the above mentioned types of crystals are only "Model Systems". They help to better understand basic deformation characteristics of a single or two-phase material. However, the engineering materials in practical use are polycrystalline and their overall mechanical behavior arises as a result of the basic considerations suggested earlier, although the overall picture will be more complicated.

The aim of this investigation is to study the deformation behavior of polycrystalline two-phase alpha-beta brass. The present study is divided into two parts:

a) Transmission Electron Microscopic (TEM) study of the deformation structure in alpha-beta brass.

b) Finite Element Method (FEM) analysis of elasto-plastic stress-strain relationships in alpha-beta brass.

The present TEM study mainly concentrates upon the analysis of the deformation structure in the alpha phase of the alpha-beta brass. The results of this present work will be compared with the TEM studies on 70 Cu-30 Zn alpha brass performed by Karashima (10,11). The FEM analysis of alpha-beta brass is based on FEM studies performed by Jinoch *et al.* (12) and Ankem *et al.* (13.14) on alpha-beta Ti-8Mn alloy.

Alpha-beta brass is similar to a large number of two-phase alloys of engineering importance, and it is hoped that the results of this study may be applicable to various other two-phase alloy systems.

II. HISTORICAL BACKGROUND

II-A. Copper-Zinc System

a) General: The term 'BRASS' is applied to a class of alloys that consist essentially of copper and zinc. They are a very important class of commercial alloys. Their popularity is mainly due to their high corrosion resistance, good machinability, and the varying mechanical properties obtainable by changes in the composition. The Copper-Zinc phase diagram (15) is presented in Figure 1. It can be observed from this diagram that the face centered cubic (F.C.C.) 'Alpha' phase can accommodate up to about 38 weight percent zinc in solid solution. The alpha phase is fairly strong and possesses excellent ductility. Many commercial brasses are made of this solid solution and they possess good formability. 70 Cu-30 Zn Cartridge Brass is one of the many alloys that is typically alpha brass. As observed from this diagram, addition of more than approximately 38 weight percent Zn results in the appearance of a second solid solution. This phase is called 'Beta' and it differs from the alpha phase in many ways. It has a cesium-chloride (CsCl) structure and is harder and stronger but much less ductile than the alpha phase. The beta phase undergoes a modification in the arrangement of solute atoms in the crystal lattice between a temperature range of 454-468 degrees Celsius (15). The high temperature stable phase is called 'Beta' (15). It has on the average a body centered cubic (B.C.C.) A2 type

Figure 1. The Copper-Zinc Phase Diagram. (Ref: 15)

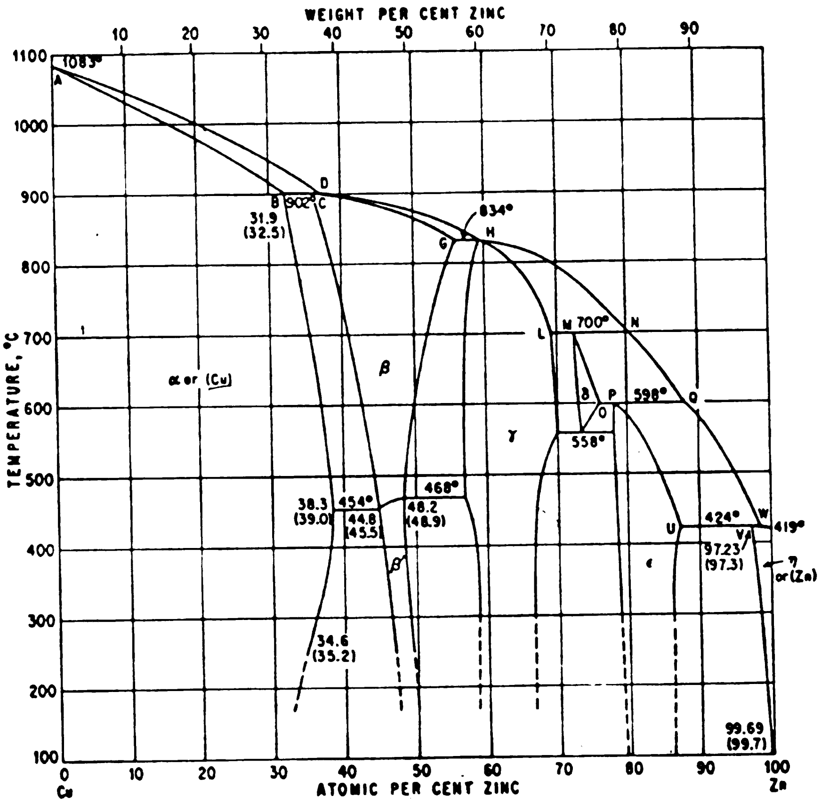
WEIGHT PER CENT ZINC
TEMPERATURE, °C
ATOMIC PER CENT ZINC
1083°
902°
834°
700°
598°
558°
468°
454°
424°
419°
31.9
(32.5)
38.3
(39.0)
44.8
(45.5)
48.2
(48.9)
34.6
(35.2)
97.23
(97.3)
99.69
(99.7)
α or (Cu)
β
β'
γ
δ
ε
η
or (Zn)
Cu
Zn

FIGURE 1.

crystal structure. On cooling below the above mentioned temperature range, the solute atoms assume an ordered cubic B2 type of structure. This low temperature form is termed as 'Beta-Prime'. The brasses varying in composition from 38 to 46 weight percent Zn, contain both alpha and beta phases. These are termed as the two-phase alpha-beta brasses. This family of brass is the main focus of this study. Brasses containing approximately 46 to 50 weight percent Zn contain the beta phase only. The brass alloys in this composition range do not find much commercial application as they are hard and brittle. With the zinc content approximately greater than 50 weight percent, a very hard brittle 'Gamma' phase appears. Alloys containing the gamma phase are useless in engineering applications.

b) Alpha-Beta Brass: Brass containing 60 weight percent Cu, 40 weight percent Zn is representative of this class, and is commonly called as 'MUNTZ METAL'. Muntz metal finds extensive use in the manufacture of pipes, tubes, and general purpose castings (16). This alloy has relatively poor cold drawing and forming properties as compared to other copper alloys, but has excellent hot working properties. It is the strongest of the commercially used Cu-Zn alloys. The typical mechanical properties of this alloy are listed in Table 1. The typical metallurgical properties of this alloy are listed in Table 2 (16).

TABLE 1

Typical Mechanical Properties of MUNTZ METAL (Ref. 16)

Yield strength:	15×10^4 - 38×10^4 KPa
Tensile strength:	37×10^4 - 51×10^4 KPa
Shear strength:	28×10^4 KPa
Percent Elongation:	10 - 52%
Modulus of Elasticity:	1.03×10^8 KPa
Modulus of Rigidity:	3.86×10^7 KPa

Note: 1 psi = 6.895 KPa

TABLE 2

Typical Metallurgical Data of MUNTZ METAL (Ref. 16)

Microstructure:	Two Phase Alpha and Beta.
Crystal Structure:	a) Alpha phase: A1 type face-centered cubic. b) Beta phase: (1) High temperature beta phase has A2 type body-centered cubic structure. (2) The low temperature beta prime phase has B2 type Cesium-Chloride (CsCl) structure.
Metallography:	Beta phase appears dark when etched with ferric chloride, and golden yellow when etched with ammonium chloride.
Liquidus Temperature:	1178°K
Solidus Temperature Range:	698 -873°K
Hot-working Temperature Range:	898 -1073°K

II-B. Two-Phase Material Investigations

a) General: Unckel (17) was one of the first to investigate deformation in polycrystalline two-phase materials. In his investigations, alloys of copper containing 6 weight percent iron, leaded brass, alpha-beta brass, complex brass (60 Cu-40 Zn brass with additions of Al, Fe, Mn, Sn, and Ni) and alpha-delta bronze were deformed by cold-rolling. The particle size was measured before and after rolling. For materials in which the second phase was softer than the matrix, like leaded brass, the amount of reduction undergone by the particles on rolling was greater than the reduction of the specimen as a whole. In all the other alloys, the inclusions were harder than the matrix, and the second phase particle deformed less than the matrix. Unckel (17) reported that as the amount of deformation is increased, the deformation of the matrix and particles tended to become more and more homogeneous, i.e. the hard particles deformed more and the soft particles deformed less. This can be attributed to the work-hardening of the softer matrix phase. Chao and Van Vlack (18) confirmed Unckel's conclusions that the extent of the deformation of the second phase depends upon the relative hardness of the particles of second phase as compared to that of the matrix.

The first detailed metallographic study of two-phase materials was undertaken by Honeycombe and Boas (19). They studied deformation behavior of alpha-beta brass and observed that during deformation, slip first appeared in alpha grains which became heavily deformed before slip was observed in the beta grains. When a heavily deformed specimen was repolished and restrained, slip lines started again in the alpha phase. Slip lines occasionally crossed the alpha-beta phase boundary. The orientation relationship between the alpha and the beta phase for this to occur was {110} in beta parallel to {111} in alpha as well as <111> in beta parallel to <110> in alpha. Honeycombe and Boas (19) also noted that more deformation occurred in the region of the beta phase near an alpha-beta boundary than in the interior of the beta grain. Clarebrough (20) subsequently studied silver-magnesium alloys which consisted of soft silver rich grains of F.C.C. alpha phase and grains of hard beta phase having a CsCl structure. These alloys deformed in a manner similar to two-phase alpha-beta brass. Studies indicated that below 30 volume percent of beta phase, the alpha phase deformed more than the beta phase. When the volume fraction of the beta phase exceeded 30 volume percent, the extent of deformation in both the phases were the same and equal to that of the alloy as a whole. Clarebrough and Perger (21) observed similar behavior in alloys of copper and zinc. Honeycombe and Boas (19) have shown that, in alpha-beta brass, preferential deformation of the softer alpha phase can occur. Mechanical properties of ductile materials containing either soft or hard particles have also been studied by Gurland (22) using different silver alloys. From his studies Gurland concluded that the type of second phase particle is not an important parameter for overall deformation characteristics so long as it does not deform during deformation of the alloy. He also suggested that, the effect of the strong second phase particle on strengthening is due to the restriction of plastic deformation of the softer matrix by the particles (22). Slip is initiated in the matrix by the stress concentrations caused by the presence of hard particles during loading. Margolin, Farrar and Greenfield (23) have studied the deformation of alpha-beta titanium alloys. In these alloys the alpha phase was distributed either as equiaxed alpha, in an aged beta matrix or as widmanstätten plates and grain boundary alpha in an aged beta matrix. For specimen with approximately same value of yield stress, the fracture strength of equiaxed alpha structure was found to be higher than that of the widmanstätten structure of the same grain size. Correspondingly, the reduction of area was higher for specimens with the equiaxed structure as compared to those with widmanstätten structure.

All the studies that have been discussed so far have been carried out using bulk polycrystalline two-phase materials (17-23). To understand the process of deformation in two-phase materials, the role of the phase boundary during the deformation needs to be investigated. Investigations using Model Systems of two-phase materials are reviewed in the following section.

b) Investigations Using Model Systems: Model Systems such as bicrystals and duplex crystals have been used to understand the basic mechanisms of deformation in two-phase materials. To study the mechanical properties and deformation mechanisms of two-phase materials, the number of variables must be minimized. The ideal fundamental unit for studying the mechanical behavior of two-phase material would be a single crystal of one phase joined to a single crystal of another phase. Such a unit is called a two-phase bicrystal (1). A duplex crystal has been defined as an oriented crystallographic unit consisting of two phases with a definite crystallographic orientation relationship with each other (3). Eberhardt *et al.* (24) have developed a method for producing two-phase alpha-beta brass bicrystals by diffusion bonding. The interface boundaries of these bicrystals are neither sharp nor stable. Bicrystals produced by such a method are in a metastable state, since they are obtained by ice-water quenching (25). Takasugi, Izumi and Fat-Halla (25-28) tested such diffusion bonded isoaxial specimens of alpha-beta brass at specific strain-rates, at various temperatures. Under such loading conditions, the strains in the alpha and beta phases are the same, and the boundary does not experience any stress. Hingwe and Subramanian (1) have developed a technique for producing bicrystals and duplex crystals of alpha-beta brass by using specialized heat-treatment schedules. The phase boundaries in bicrystals grown by them are extremely sharp (< 1μm thick) and are stable, similar to that in actual two-phase materials. Studies on alpha-beta brass by Hingwe and Subramanian (2) employed a series type bicrystal where the phase boundary was normal to the tensile axis. Under such loading, alpha phase, beta phase and the boundary experience the same stress due to the external load.

Under any general state of stress, macroscopic and microscopic compatibility conditions must be satisfied at the grain boundary (3). For an isoaxial, symmetric bicrystal, consisting of crystal 'A' and crystal 'B' (see Figure 2), with the planar boundary normal to the Y-axis, the macroscopic compatibility conditions that must be satisfied are:

$$\left[\epsilon_{xx}\right]_A = \left[\epsilon_{xx}\right]_B \quad ; \quad \left[\epsilon_{zz}\right]_A = \left[\epsilon_{zz}\right]_B \quad ; \quad \left[\epsilon_{xz}\right]_A = \left[\epsilon_{xz}\right]_B \qquad (\underline{\text{II}}\text{-}1)$$

where, ϵ_{xx} , ϵ_{zz} and ϵ_{xz} are strain components and subscripts 'A' and 'B' represent the regions in the crystal 'A' and 'B', respectively. In addition, the strain in the loading direction in crystal 'A', $\left[\epsilon_{zz}\right]_A$, should be equal to the strain in crystal 'B', $\left[\epsilon_{zz}\right]_B$, and these two in turn should be equal to the total strain, ϵ_{zz} , of the bicrystal. These compatibility relations can become incompatible in an anisotropic crystal. Compatibility conditions are more complicated in a polycrystalline aggregate.

Figure 2. Schematic of a bicrystal consisting of crystals 'A' and 'B'. Loading is along the Z-direction.

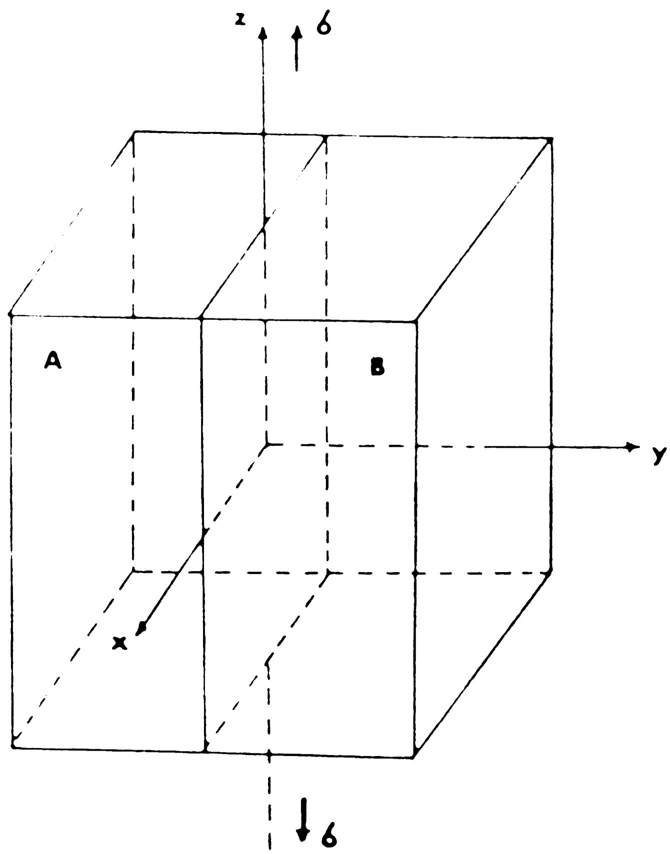

FIGURE 2.

Hingwe and Subramanian (2) deformed bicrystals of alpha-beta brass in uniaxial tension to study the initiation of plastic deformation and its propagation across the phase boundary. The effectiveness of the phase boundary as a barrier for slip propagation depends upon the relative crystallographic orientation of the two phases. Slip was observed in the beta phase only after secondary slip and cross-slip took place in the alpha phase. This may be due to:

1) The difference in the shear moduli of the alpha and beta phase or,

2) Difference in the Burgers vector of slip dislocation in the two phases, or

3) Difference in the number of available slip systems (2).

Nilsen and Subramanian (5) have carried out tensile-tests on bicrystal specimens of alpha-beta brass at various strain-rates, and for specimens having two different types of boundary geometries, corrugated and flat. According to them, the corrugated boundary was more effective in blocking the propagation of slip from alpha to beta phase. All specimens tested were found to be strain-rate sensitive. At low strain-rates, both boundaries were ineffective barriers, and coarse slip was observed in the alpha phase. Fine slip was observed at high strain-rates in the alpha phase. Slip propagation in the beta phase requires the movement and multiplication of superlattice dislocations. These superlattice dislocations are composed of two perfect dislocations joined to one another by an antiphase boundary. Since the dislocations are connected to one another by an antiphase boundary, they must move as a single unit. As a result, their motion is difficult and requires a high stress. As any slip line crosses from the alpha phase into the beta phase, it will proceed only to a limited extent. This extent depends upon the level of stress concentration created in the alpha phase near the phase boundary. The effect of this stress concentration in the beta phase diminishes in direct proportion to the distance from the phase boundary. When the slip line reaches a position at which the stress concentration is insufficient to continue the propagation, it will stop. Nilsen and Subramanian (4) have also carried out investigations on bicrystals of alpha-beta brass consisting of oriented and equiaxed duplex boundaries. Equiaxed boundaries were found to be more effective in blocking the propagation of deformation from alpha to beta phase, than the oriented boundary. Nilsen and Subramanian (4,5) concluded that wider slip bands formed in alpha phase produced a more effective stress concentration so as to activate slip in beta phase across the boundary. Fine or multiple slip formed in alpha phase at high strain-rates, did not produce effective stress concentrations to cause slip across the boundary. High strain-rate, produces fine slip in alpha phase by activating many dislocation sources.

Interaction of fine slip with the boundary causes multiple slip which immobilizes a large fraction of the dislocations. Kezri-Yazdan and Subramanian (29) have studied the role of phase boundary orientation relative to the tensile axis in bicrystals of alpha-beta brass. Under such a geometry, the phase boundary experiences both shear and normal stresses during loading. It was found that in the bicrystal specimens having inclined boundaries, the interaction of slip in the alpha phase with the phase boundary was not the motivating force for creating deformation in the beta phase. In these specimens, the slip in the beta phase normally occurred on its own. This may be due to the shear stresses acting on the inclined boundaries.

Fat-Halla *et al.* have studied operative slip systems in diffusion bonded alpha-beta brass two-phase bicrystals at 150°K. Their studies showed that the primary $(111)[\bar{1}01]$ system was operative in the alpha phase and P_β $[111]$ system was operative in the beta phase, where P_β is the actually observed slip plane in the beta phase lying between $[\bar{1}01]$ and $[\bar{1}\bar{1}2]$. Fat-Halla *et al.* (30) have also studied the elastic incompatibility of isoaxial bicrystals of alpha-beta brass during deformation. Kawazoe *et al.* (31) have also performed fatigue tests on diffusion bonded two-phase bicrystals of alpha-beta brass. The fatigue tests were performed at 30 Hz in tension and compression, under a constant stress amplitude of about

± 100 MPa. Predominant slip in the alpha phase occurred on the primary (111) plane, while that in beta phase occurred on planes apart from $(\bar{1}01)$, rather close to $(\bar{2}11)$. Interface studies by Takasugi and Izumi (32) on bicrystals of alpha-beta brass led them to believe that the phenomenon of interface sliding was strongly dependent upon the nature of the interface, the orientation relationships, the shear direction and the microstructure of the interface.

Margolin and co-workers (33-38) have published a series of papers on the deformation behavior of beta brass using beta brass bicrystals. Chuang and Margolin (33) studied the stress-strain relationships of beta brass bicrystals. Three isoaxial bicrystals and one non-isoaxial bicrystal of beta brass, oriented to have the grain boundaries parallel to the axis of loading were used in their studies to investigate the stress-strain relationships. It was found that grain boundary strengthening was greater in non-isoaxial bicrystals of beta brass. Lee and Margolin (34) studied the stress-strain behavior of beta brass using bicrystals and tricrystals of beta brass. Their studies showed that the flow-stress in the bicrystal specimens was higher than the single-crystal flow-stress at the same strain level, whereas the tricrystal flow stresses were only slightly higher than those of bicrystal specimens at the same strain level. Secondary stresses in tricrystals had a slower decay rate than in bicrystals. Based on this observation, Lee *et al.* have suggested that the secondary stresses would spread across a grain more rapidly in a polycrystalline material, where the constraints are the highest (34). The average grain boundary stress in tricrystals was found to be smaller than the corresponding stress for bicrystals despite the increased constraint. Lee and Margolin (35) have also studied the effective Young's modulus in isoaxial bicrystals and tricrystals of beta brass. Studies showed that the slope of the elastic portion of the stress-strain curve of bicrystals was markedly higher than that of its component crystals. The increase in slope of tricrystals was only slightly higher than the bicrystal specimen. These changes in slopes arise due to the elastic shear incompatibility at the grain boundary. The apparent elastic modulus of some bicrystal grain boundaries was found to be higher than that of the beta grain interior. Margolin *et al.* (36) showed that, if examined separately, the grain boundary and the grain interior possess separate and different stress-strain relationships. Yaguchi and Margolin (37) have also studied the grain boundary contribution to the Bauschinger effect in beta brass bicrystals. Their studies revealed that at similar strain levels in the grain boundary and the grain interior, the former unloads faster due to its higher modulus than the latter. Thus Yaguchi *et al.* (37) suggested that at overall zero stress level, the grain boundary experiences compression and the grain interior experiences tension. After prior tensile straining, if the specimen is compressed, the grain boundary will yield first (37). Yaguchi and Margolin (38), from their studies, have shown that the flow in the twinning direction of the bicrystal required a higher stress than flow in the anti-twinning direction, and prior slip in compression raised the stress required for flow in tension.

c) Plastic Deformation and Slip

General: Plastic deformation of a crystalline material causes rapid dislocation multiplication with increasing plastic strain. In the early stages of deformation, the dislocation movement tends to be confined to a single set of parallel slip planes (6). On further deformation, slip occurs in other slip systems, and different dislocations moving in different slip systems interact. This dislocation interaction depends upon many factors such as temperature, crystal structure of the material, strain, strain-rate, inclusions or precipitates, and the nature of stacking faults (6). During the plastic deformation of a polycrystalline material, the dislocations must overcome the resistance resulting from obstacles such as impurity atoms, point defects, other dislocations and grain boundaries. Dislocations tend to pile-up at the grain boundaries (6). Because of this dislocation pile-up, a back stress is created which eventually may stop the dislocation source from operating (6). In the region where the leading dislocation is stopped at a boundary, a stress concentration will occur. If the stress concentration is high enough, the slip proceeds across the boundary and moves on a coherent slip plane in the adjacent region.

Various mechanisms have been proposed to explain the continuation of slip through the boundary into the adjacent grain (6). One possibility is that the high stress concentration preceding the leading dislocation in the slip band causes the dislocations to cross the boundary and move into the adjacent grain (39). These newly created dislocations, then under the combined action of the applied stresses and the stresses due to dislocation pile-ups at the boundary continue to glide in that region. Another theory predicts that the leading dislocations in the pile-up produce a stress concentration at the grain boundary, and this stress concentration causes some of the boundary dislocations to move into the adjacent grain (40). Another theory predicts that the stress concentration, produced by the dislocation pile-up at the boundary, activates dislocation sources present in the nearby region of the adjacent grain (41).

The decay in the intensity of slip at the boundary could according to Margolin *et al.* (40) imply that there is "elastic opposition" to the operation of slip system as the slip approaches the boundary. Hence, cross-slip according to them, becomes more favorable near the boundary (40). Resistance to plastic deformation as a result of elastic restraints of the adjacent grain and constraints at the boundary is termed as 'elastic opposition' by Margolin *et al.* (40). Elastic opposition to the operation of slip in one grain by the neighboring grain has been observed by Margolin *et al.* (40). He states that although the elastic interaction assists the nucleation of slip, plastic incompatibility opposes it. At a distance from the boundary, plastic incompatibility does not have a significant effect on the operation of slip. But as slip approaches the boundary, the compatibility effects become more prominent, causing decay of the slip intensity and the occurence of cross-slip.

Plastic Deformation Behavior of Alpha Brass: Alpha brass is a single-phase substitutional solid solution of zinc in copper. The zinc atoms, in alpha brass, occupy random substitutional atomic positions in a F.C.C. crystal lattice structure. Alpha brass usually deforms along close packed {111} planes in the $<1\bar{1}0>$ directions. Alpha brass is stronger than copper and the increase in strength of alpha brass, as compared to copper, may be attributed to the solid solution hardening caused by the addition of zinc atoms to copper (3). Presence of zinc affects both the stress necessary to initiate plastic deformation and subsequent work-hardening (3). The critical shear stress in alpha brass crystals increases linearly with the zinc concentration. Ardley and Cottrell (42) have studied the yielding phenomenon in alpha brass crystals at room temperature. Well marked yield points have been observed in virgin and strain-aged specimen. Further, both the upper yield stress and the yield drop, increase markedly with increasing zinc content (42). When an F.C.C. alpha brass single-crystal is deformed in uniaxial tension, the plot of the resolved stress as a function of the shear strain exhibits three stages of deformation, i.e. Stages I, II and III. As the zinc concentration is increased, Stage I (easy-glide region) becomes longer, Stage II (linear-hardening region) increases in range, and Stage III starts at a higher stress level. At the end of the easy-glide, the shear stress in the primary slip system, has been found to be the controlling factor in initiating secondary slip. It is assumed that easy-glide ends when the stress concentration around the clusters of dislocations on the primary slip plane is sufficiently large to initiate slip on another slip plane. In case of alpha brass, higher stress concentration is required to initiate secondary slip as compared to other F.C.C. materials. This means that bigger clusters of dislocations are required on the primary slip planes; this can be achieved by a long easy-glide.

Stacking fault energy is one of the parameters that is important in determining whether cross-slip is possible. Lowering the stacking fault energy widens the separation between the partial dislocations. Widening the separation of partial dislocations makes cross-slip difficult.

however, sometimes pile-ups of dislocations in the primary slip plane lead to the activation of nearby sources on the cross-slip planes. Hence cross-slip in alpha brass can take place in spite of its low staking fault energy (43). Karashima (10) has studied the dislocation structure in deformed alpha brass using Transmission Electron Microscopy. He observed that at low strains (1-5 percent) dislocations piled-up against the boundary and at obstacles within a crystal. It was also observed that with increasing degree of deformation (5-10 percent), dislocations from two or three slip systems interacted to form dislocation tangles and kinks. A prominent characteristic of alpha brass is that most of the dislocations introduced during cold-working are confined to the primary slip planes. This behavior is quite different from that found in metals having a high stacking fault energy like beta brass (10). Karashima's studies showed that slip progresses through grain boundaries and twin boundaries, with a clear indication that slip was continuous across the boundary into the neighboring grain. Slip can be induced into the neighboring grain with the aid of stress concentration from the pile-ups of dislocations against the grain boundary (10). Such a pile-up can activate dislocation sources present in the neighboring grains or make the grain boundary dislocation sources operative. Mitchell and Thornton (44) have investigated the role of secondary slip during deformation of copper and alpha brass single crystals. Secondary slip is likely to be important during Stage II of deformation. They have found that with increasing zinc content the amount of secondary slip decreases (44).

<u>Plastic Deformation Behavior of Beta Brass:</u> Beta brass is an intermediate solid solution of the Cu-Zn system. The ordered beta prime phase has a cesium-chloride structure, which is equivalent to two interconnected simple cubic unit cells; one of copper and the other zinc. This type of structure is referred to as the B2 type superlattice. Beta brass normally deforms by slip on {110} planes and in $\langle 1\bar{1}1 \rangle$ directions and in general is a material having high stacking fault energy. In the ordered state, the dislocation behavior of the beta prime phase is different from that of the disordered B.C.C. beta phase. A slip vector displacement causes an atom in one layer to move from one position to a new position at a unit distance. This produces a change in the local arrangement of the atoms on the slip plane, thereby creating an antiphase boundary (6). This boundary has a specific energy, depending upon the degree of order in the lattice. This disorder produced by the slip process, can be removed by a second dislocation, which restores the original atomic arrangement. Thus a perfect dislocation in an ordered lattice consists of two ordinary dislocations on the slip plane joined by an antiphase domain boundary (45). This is similar to an extended dislocation consisting of two

partial dislocations joined by a stacking fault (45). Since single unit dislocation produces an antiphase domain boundary, it is energetically favorable for it to be associated with a second unit dislocation which removes the high energy fault. This pair of dislocations are called superlattice dislocations, and move on the same slip plane in the crystal. A high stress, however, is required to move these superlattice dislocations (46).

Two distinct structural characteristics, namely slip bands and deformation bands, have been observed in deformed beta brass (47). Slip lines in beta brass are less prominent than those in F.C.C. metals (47). Both temperature and mode of deformation have been found to affect the occurence and spacing of deformation bands (47).

Because of the highly anisotropic nature of beta brass, the electron microscope contrast theory based on isotropic invisibility criteria fails, except for pure edge or pure screw dislocations (46). Head *et al.* (48) have computed the theoretical image profiles of dislocations according to the two-beam dynamical theory, and considering the full anisotropic strain fields of the dislocations (48). Comparing the character of the theoretically predicted and experimentally observed dislocation images, they have concluded that the majority of dislocations in beta brass are screw dislocations of type a<111> gliding on $\{\bar{1}10\}$. Some of these a<111> dislocations split into two a/2<111) dislocations. Other dislocations are of a<010>

type glissile on {001}.

Elastic properties of cubic crystals are governed by values of three elastic stiffness constants (C_{11} , C_{12} and C_{44}) and the elastic compliances (S_{11} , S_{12} and S_{44}) (49). The displacement field around a dislocation, and the electron diffraction contrast from the dislocation, involve only ratios of these constants:

$$A = \frac{2C_{44}}{C_{11}-C_{12}} = 2\frac{S_{11}-S_{12}}{S_{44}} , \qquad (\underline{II}-2)$$

$$B = \frac{C_{11}+2C_{12}}{C_{44}} = \frac{S_{44}}{S_{11}+2S_{12}} . \qquad (\underline{II}-3)$$

A value of 'A' = 1 ('A' is called the Zeners constant) indicates that the material is isotropic. In that case the constant 'B' is related to the Poisson's ratio (ν) by:

$$B = \frac{2(1+\nu)}{1-2\nu} . \qquad (\underline{II}-4)$$

Materials having an 'A' value much less or greater than one are termed as highly anisotropic. Of the commonly known materials beta brass has one of the highest values of 7.8 and thus is highly anisotropic (49).

In an elastically anisotropic material like beta brass, the energy of a dislocation depends upon the crystallographic orientation of the dislocation line (50). A straight dislocation which is in a high energy state may be unstable and its energy decreases if it changes to a zig-zag shape. In elastically isotropic crystals, with no applied stress, the equilibrium position of a dislocation running between two pinning points is along a straight line joining the two pinning points. Dewitt and Koehler (51) have shown that this is not a necessary condition in an elastically anisotropic material. In such materials, the straight dislocation can be in an unstable equilibrium. Its total energy may decrease by bowing out, even though its length will increase, since the dislocation then lies in the direction of lower energy. Head (50) has reported that the typical unstable dislocations in beta brass appear to be V-shaped. Many Z-shaped dislocations and higher order zig-zags have also been observed (50). Isotropic elasticity would be a very poor approximation for dislocations in beta brass. For any Burgers vector, a dislocation in an isotropic medium has an energy ratio of edge to screw of $1/1-\nu$. Since typically $\nu = 0.3$, this energy ratio is 1.5. For beta brass, this ratio varies from 3.6 to 0.51. So it is impossible to choose a single value of Poisson's ratio for beta brass, which would adequately describe the dislocation energy relationships. So for beta brass, it is misleading to use isotropic approximations to determine dislocation energies, or those quantities that depend directly on the dislocation energy, such as the direction of dislocation line and force between parallel dislocations.

In beta brass, the elastic invisibility criteria, such as $\vec{g} \cdot \vec{b} = 0$ and $\vec{g} \cdot \vec{b} \times \vec{u} = 0$, where $\vec{g}$ is the diffracting vector, $\vec{b}$ the Burgers vector, and $\vec{u}$ the vector along the dislocation line are not valid in general, except for pure screw or edge dislocations lying perpendicular to a symmetry plane of the crystal (52). In general it is extremely difficult to put a dislocation out of contrast in beta brass (52). Therefore, the usual relations for this condition, i.e. $\vec{g} \cdot \vec{b} = 0$ and $\vec{g} \cdot \vec{b} \times \vec{u} = 0$, could not be identified. Head *et al.* used a computer image matching technique to determine the Burgers vectors of less complex and straight dislocations in beta brass. A majority of the dislocations seemed to lie close to <111> direction. Such dislocations of screw orientation have a Burgers vector of a<111>. Two of the most characteristic TEM dislocation contrast effects observed in beta brass by Head *et al.* were:

1) <111> dislocations showing double images when using either a [110] or a [112] reflection perpendicular to the dislocation line, and
2) Markedly dotted appearance of dislocation images in the [110] reflection.

Observation of paired-dislocations of Burgers vector of a/2<111> has also been reported by Head *et al.* (48). It has been suggested that these like dislocations of Burgers vector a/2<111> together may constitute a superlattice dislocation of a<111> separated by a small region of disordered material. Head *et al.* (48) have reported that the slip system <010> {101} is also operative in some cases in beta brass. Dislocations of Burgers vector a<100> were found to be glissile on {100}.

II-C. Finite Element Method

An important part of the present investigation involves using a continuum mechanism approach with the help of Finite Element Method (FEM) analysis to analyze the elasto-plastic deformation behavior of alpha-beta brass. FEM analysis was used in this present investigation to determine the stress-strain levels in the alpha and beta phases and in regions near the boundary during loading.

FEM is an approximate numerical method which can be effectively used for solving various problems of stress analysis in engineering (12). The solution of a continuum mechanics problem is approximated by polynomials on simple areas called "Finite Elements". The area of the problem is divided into these finite elements. The values of the solution at the nodes of the finite element mesh, are determined by solving a large system of linear algebraic equations, assembled into a matrix operation. These equations represent physical quantities or parameters specific to the given problem. The division of the total area into elements is fairly arbitrary and each element may have different material properties, linear or non-linear. With the necessary input data, FEM can be used to study mechanical behavior of multi-phase alloys, provided the stress-strain behavior of the individual phases are known or can be approximated. Zienkiewiez (53) has given a thorough treatment of the theory and application of FEM.

The use of FEM to investigate metallurgical problems has been described by Swedlow and Smelser (54) as an "opening in the traditional wall between mechanicists and metallurgists." One of the first so called "openings in the wall" was made by Fischmeister *et al.* (55). They used FEM to study plastic deformation of two-phase materials. They applied FEM analysis to plain-carbon (0.21 percent carbon) steel and calculated the stress-strain curves for different hardness ratios of the ferrite and martensite phases. They studied deformation in the individual phases by using a two-dimensional "plate" model of the ferrite-martensite microstructure. This model was obtained by subdividing each phase region of the microstructure into triangular elements. The deformation of all the phase regions was calculated for a plane strain and linear work-hardening condition in both phases. Both phases were assigned identical values of Young's modulus and work-hardening rates. Sundström (56) studied the elastic-plastic behavior of tungsten carbide-cobalt (WC-Co) composite using FEM. The aim of his investigation was to ascertain whether FEM could be applied to predict elastic-plastic behavior of a two-phase material. His investigations showed that continuum mechanics applied to a two-dimensional model of real microstructure comprising of 20-30 grains gives a reasonable agreement with the experimental stress-strain curves at low stress levels. However, he concluded that the plastic strain distribution calculated by FEM is very inhomogenious at the microscale.

Secondly, FEM cannot give a very high resolution on the microscale of stress and strain fields in the phases. The reason for it, according to Sundström, lies in the computational limitations leading to a relatively coarse sub-division of the model into elements. Mean values of the field quantities over the critical region, however, gives information about the interaction between phases. According to Swedlow and Smelser (54), FEM analysis tends to be "overstiff". It generates low strains for a given stress level or excessive stress at a given strain level.

From the theory of elasticity it is known that there is a similarity in the solutions of two and three-dimensional mechanics problems with equivalent geometry. This resemblance can also be found in the plastic range if one considers the two-dimensional problem under plane strain condition (12). Physically, the assumption of plane strain means that there is a strong constraint to the plastic flow perpendicular to the plane of the two-dimensional plate. Therefore, it is assumed that the two-dimensional model gives a fair description of the real three-dimensional structure.

All materials are anisotropic on the grain size level. FEM assumes isotropy for all the phases. However, if there is a large difference in the elastic moduli values between the phases, the influence of anisotropy of the phases is then diminished, thus justifying the assumptions of isotropy. Also, the FEM model is not the truest representation of the volume fractions and the distribution of phases in the bulk material. Limitations in the calculation capacity determine the number of elements available for the model. Karlsson and Sundström (57) used FEM to study inhomogeneiety in plastic deformation of two-phase steels. In their investigation, the FEM analysis was performed on the ferrite and martensite microstructure of an alloyed low-carbon steel using constant strain elements. Their investigations revealed that a very inhomogenious strain distribution exists in two-phase structures. The inhomogeneity is strongly dependent upon the hardness ratio of the two phases. Maximum strains were found to appear away from the interfaces.

Margolin *et al.* (12,13,14) published a series of three papers on deformation studies on alpha-beta Ti- 8Mn alloy using FEM. The first of these studies, performed by Jinoch, Ankem and Margolin (12), analyzed stress-strain curves of alpha-beta Ti- 8Mn alloy using stress-strain curves and approximate volume fractions of each phase. Stress distributions in the two phases were numerically calculated in their studies using an IBM 360/65 computer by means of a finite element NASTRAN program developed by NASA. They used a uniform mesh of 392 triangular elements for the FEM analysis. Sub-areas of alpha phase were located by projecting a photo-micrograph onto a graph of the size of the entire mesh. The alpha particle shapes were idealized to make calculations simpler while maintaining volume fractions of alpha phase constant at 17 percent. Their investigations revealed that the FEM calculated stress-strain curve lies below the experimental one. The reason for this is attributed to the fact that the beta grains and the alpha particle sizes in the Ti -8Mn alloy were smaller than the single phase alpha and beta grain sizes in the alloy whose stress-strain curves were used in the FEM calculations. Secondly, the role of the interface could not be discarded, or ignored, in a two-phase alloy. Jinoch *et al.* (12) also investigated stress distribution in the alpha-beta phases of the Ti -8Mn alloy. Stress gradients were found to be present in both phases. In the beta phase, stresses were higher near the interface, and in some instances, this was found to be true in the alpha phase as well. For stresses below those producing plastic strain, the strain in alpha phase were higher than in the beta phase.

Ankem and Margolin (13,14) have presented a two-part analysis of FEM calculations of stress-strain behavior of alpha-beta Ti- 8Mn alloys. Part I dealt with the determination of stress-strain relations and Part II with the stress-strain distributions. They used the NASTRAN computer program (developed by NASA) to calculate the effect of particle size, matrix and volume fractions on the stress-strain relations of alpha-beta Ti- 8Mn alloys. For a given volume fraction, the calculated stress-strain curve was higher for a fine grain size than for a coarse grain size. When the stronger beta phase was the matrix, stress-strain curves reached higher stress values. They also concluded that the difference in the calculated and experimental curves diminished at higher strains. Their investigations did not consider anisotropy of alpha and beta phases either in their elastic or plastic state. Also, no distinction was made between slip behavior in equiaxed and widmanstätten alpha phase. Investigations also revealed that the average strains in the alpha phase were higher than the average strains in the beta phase. Values of strains were higher in the alpha phase than in the beta phase. The maximum value of strain in the alpha phase appeared at the center of the particle away from the constraints imposed by the beta phase. Maximum strains in the beta phase appeared at the alpha-beta interface. The longitudinal stresses, in the tensile direction, were higher in beta phase.

In this work, the above mentioned investigations by Margolin and associates have been used as a basis for the FEM analysis of alpha-beta brass (12,13,14). The theoretical and experimental procedure used is described in detail in the following chapter.

III. EXPERIMENTAL PROCEDURE

III-A. Transmission Electron Microscopic Study of the Deformation Structure

Large grained polycrystalline specimens of alpha-beta brass were used for the present study to aid in the TEM observations. The large grained specimens used in this study were prepared by using the following procedure. The available stock was rolled down to a thickness of about 1mm using a cold-rolling mill. Tensile specimens of 15mm gauge length and 7mm width were cut from them. These tensile specimens were then annealed for 1-hour at 425 degrees Celsius under a charcoal cover to relieve any prior stresses induced in the material. The annealed tensile specimens were then subjected to a strain-annealing treatment to obtain a large grain size of about 0.5-1.0mm for this study. The annealed specimens were first deformed in tension to a critical strain of 8 percent, using a micro-tensile testing device attached to an Instron machine. These strained specimens were then heat-treated at 825 degrees Celsius for 72-hours in evacuated quartz tubes to obtain the large grain size. These large grained heat-treated specimens of alpha-beta brass were then subsequently strained to the order of 5 percent and 8 percent plastic strains, using the micro-tensile testing device mentioned earlier. The strain levels were chosen in order to induce definite amounts of plastic strain in the specimens. These deformed specimens were then chemically thinned down to 0.20mm using a solution of 60 volume percent distilled water and 40 volume percent nitric acid. The thinned specimens were washed with methanol. Three millimeter diameter discs were then cut out from the gauge length of the thinned specimens, using a very sharp pair of scissors to minimize the damage from the cutting operation. The central portion of the 3mm discs were made transparent to an electron beam by using the following two-step polishing process.

The first step, the conditions for which are given in Table 3, is known as the 'Dishing Technique' (58). It was used to produce a preferential polishing in the central region of the specimen using a funnel-shaped apparatus shown in Figure 3. After polishing the 3mm specimen for abut one-half minute, the specimen was turned over and polished on the other side as well. The 'Dishing Technique' or 'Jet-Polishing' created a shiny disc-shaped concave surface in the central part of the specimen. The main aim of producing concave-shaped surfaces on both sides of the specimen was to produce conditions suitable for causing perforation in the central region of the specimen, during the second step of the polishing process.

In the second step, the 'dished' specimen was held between circular platinum loops as shown in Figure 4 and electro-polished under conditions described in Table 4. The cathode during this electro-polishing step was a cylindrical stainless-steel sheet with slots cut out of it.

Figure 3. Schematic of 'Jet-Polishing' unit. (by courtesy of S. Shekhar, MMM, Michigan State University).

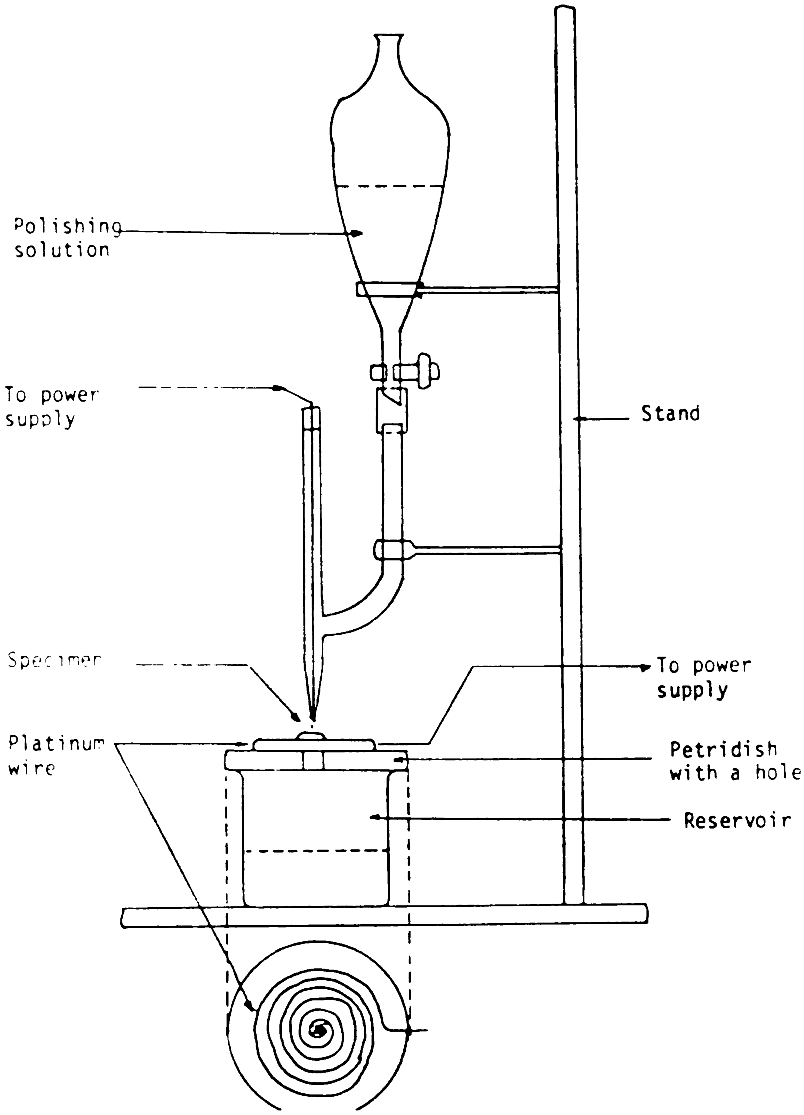
Polishing
solution
To power
supply
Stand
Specimen
To power
supply
Platinum
wire
Petridish
with a hole
Reservoir

FIGURE 3.

TABLE 3

Electropolishing data for "Dishing Technique".

Composition of Electrolyte	Voltage	Temperature
4 parts of Methyl Alcohol plus 1 part of Nitric Acid	50 volts (d.c.)	243 °K

(by courtesy of S Shekhar, MMM, Michigan State University)

Figure 4. Schematic of the final electropolishing unit. (by courtesy of S. Shekhar, MMM, Michigan State University).

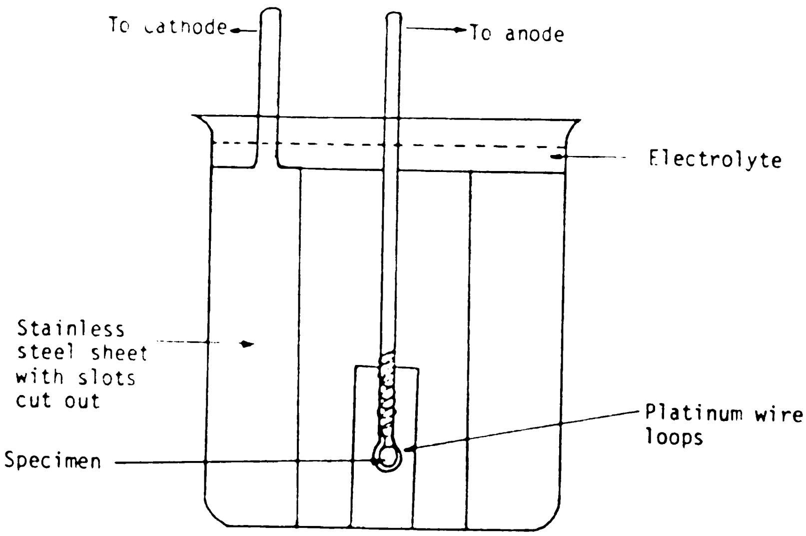
To cathode
To anode
Electrolyte
Stainless steel sheet with slots cut out
Platinum wire loops
Specimen

FIGURE 4.

TABLE 4

Electropolishing Data for Final Step of Thin Foil Preparation.

Composition of Electrolyte	Voltage	Temperature
4 parts of Methyl Alcohol plus 1 part of Nitric Acid	8 volts (d.c.)	243 °K

(by courtesy of S Shekhar, MMM, Michigan State University)

A pointed light source was used to determine when perforation occurred in the central portion of the specimen. The final electro-polishing time was about 1-3 minutes, and as soon as the hole was formed in the center of the specimen, the specimen was removed from the electrolyte and washed thoroughly in running methanol for at least 7-10 minutes. These large grained specimens of alpha-beta brass were then examined in a conventional Transmission Electron Microscope, operated at 100KV.

III-B. Finite Element Analysis

The numerical calculations for the FEM analysis were carried out on the PRIME 750 computer system by means of the ANSYS Engineering Analysis Computer Program developed by Swanson Analysis Systems, Inc. The earlier part of this section deals with the important features of the ANSYS Computer Program. A description of the procedure adopted to analyze the stress-strain relationships and stress-strain distributions in alpha-beta brass using the ANSYS program is presented in the latter part of this section. The analysis capabilities of the ANSYS Computer Program (59) include; static and dynamic analysis, elastic, plastic, creep and swelling, buckling and deflection, study and transient state heat transfer, and fluid and current flow. The program is capable of analyzing two- and three-dimensional frame structures, piping systems, two-dimensional plane and axisymmetric solids, three-dimensional solids, flat plates, shell structure and other non-linear type problems.

The ANSYS Computer Program uses a "WAVE FRONT" (or FRONTAL) direct solution method (59). It can give a highly accurate result in a minimum amount of computer time. The number of equations that are active after any element has been processed during the solution is called the "wave-front" at the point. The present problem at hand is solved using three phases:

1) Pre-processing phase,

2) Solution phase, and

3) Post-processing phase.

The ANSYS pre-processor routine contains powerful mesh-generation capabilities, as well as, capabilities to define the material properties, material constants, and loads. The solution routine formulates the element matrices, performs the overall matrix triangularization and also computes the displacement, stress and other field parameters. The post-processing routines can plot geometries, stress contours, temperature contours, stress-strain curves, time-history graphs. The ANSYS element library (59) offers 95 different element types to carry out a wide range of engineering analyses. For the stress-strain analysis of alpha-beta brass, element type 42, termed as STIF 42, was used (59). STIF 42 is used for problems involving two-dimensional isoparametric problems. 'STIF 42' (59) is used for two-dimensional modeling of solid structures. The element can be used as a biaxial plane element (plane stress or plane strain) or as an axisymmetric ring element. The element is defined by three or four nodal points having two degrees of freedom at each node, i.e. translations in nodal X- or Y-directions. The STIF 42 element (59) has plastic, creep, swelling, stress stiffening, and large rotation capabilities.

The solution printout from a full execution run using the ANSYS program (59) consists basically of two parts:

1) Nodal solution, and

2) Element solution.

The Nodal solution gives the displacements at each node of the finite element mesh. The element solution gives the normal stresses in each element, the three principal stresses, plastic and elastic strains in each element and a large amount of other additional stress-strain data.

For plastic analysis, the non-linear properties of the material have to be defined (59). All materials are assumed to be isotropic. ANSYS uses the Initial Stress Approach (59), also described as the Residual Strain Method for analyzing plasticity effects. This procedure defines a reference elastic material stiffness with corresponding reference elastic strains. Any departures from linearity are treated as initial strains. The Initial Stress Approach uses an Iterative Solution Technique with a constant triangularized stiffness matrix and a changing load vector (59). Yielding is based on the Von-Mises yielding criterion. The triangularized matrix is automatically reused for each iteration. Six different types of loading behaviors can be selected. For the present analysis, the material behavior under loading was assumed to be non-linear elastic. This loading behavior is conservative, i.e. non-path dependent. It is useful for materials undergoing only loading, and no unloading. The materials under this loading behavior show no hysterysis effect.

To generate a non-linear stress-strain relationship, the Young's modulus, the Poisson's ratio, five strains in the non-linear region of the stress-strain curve, and the corresponding stresses for the five strains defined earlier, have to be specified (59). The ANSYS program assumes the stress-strain curves to be a function of temperature, i.e. the stress-strain curves are different at different temperature levels. If the temperature factor is constant, then one has to define the same stress-strain curve as if they were obtained at two different temperatures. Linear interpolation is used between the points specified on a curve and between curves of different temperatures.

This part of the present section describes the experimental procedure used to analyze the stress-strain relationships in alpha-beta brass. A uniform 'mesh' of 60 triangular elements was prepared for the analysis. The FEM analysis was performed for three different volume percents of beta phase and three different grain sizes as shown in Figures 5, 6, and 7. The beta particles were distributed uniformly in the mesh while maintaining the volume fraction constant at the appropriate level. The shapes of the particles incorporated in the mesh were not the same as those in the actual specimen. This difference could influence the calculated stress-strain behavior. Meshes in Figures 5, 6, and 7 were used for the calculation of the overall stress-strain curves. For calculations of the stress-strain distributions, the beta particles in the mesh were incorporated into a single particle while maintaining the volume fraction constant.

The stress-strain curve for alpha brass was based on the stress-strain curve of brass containing 70 weight percent copper and 30 weight percent zinc. The stress-strain curve for beta brass was extrapolated from the available values of Young's modulus, yield stress and the corresponding strain value at the yield stress level (60). The input stress-strain curves are shown in Figure 8.

In the meshes shown in Figure 5, 6, 7, node 'J' was considered fixed, and all the other nodes along $\overline{AB}$ could move in the X-direction only. All the other nodes in the mesh could move in both X- and Y-directions, except the nodes along $\overline{CD}$, which had the same Y-displacement at any stage of deformation. For generating the stress-strain curves, the applied stresses were known for each loading condition. The corresponding strains were calculated from

Figure 5. FEM mesh for alpha-beta brass containing 20 volume percent beta phase (beta phase is shaded dark):

a) Fine grain distribution.

b) Medium grain distribution.

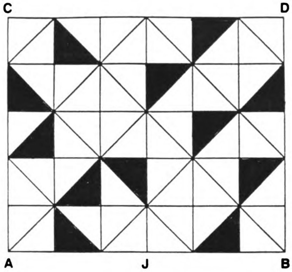

a

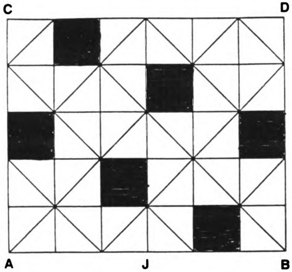

b

FIGURE 5.

Figure 5 (cont'd.).
c) Coarse grain distribution.

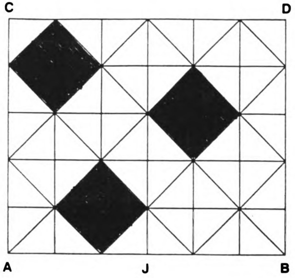

C

FIGURE 5 (cont'd.)

Figure 6. FEM mesh for alpha-beta brass containing 40 volume percent beta phase (beta phase is shaded dark):
a) Fine grain distribution.
b) Medium grain distribution.

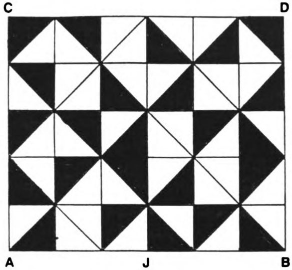

a

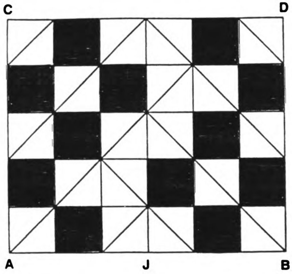

b

FIGURE 6.

Figure 6 (cont'd.).
c) Coarse grain distribution.

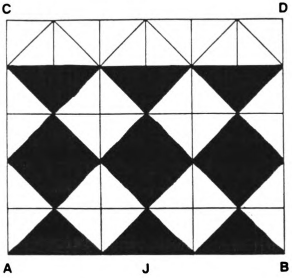

C

FIGURE 6 (cont'd.)

Figure 7. FEM mesh for alpha-beta brass containing 60 volume percent beta phase (beta phase is shaded dark):
a) Fine grain distribution.
b) Medium grain distribution.

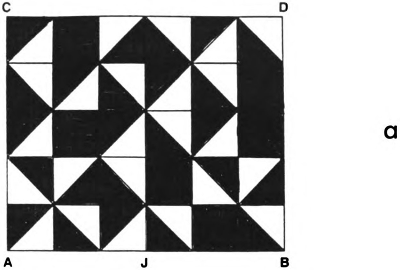

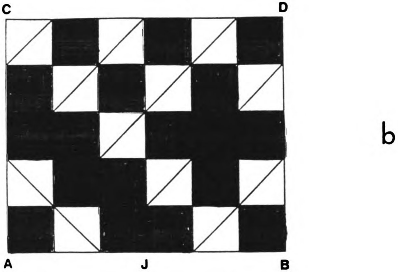

FIGURE 7.

Figure 7 (cont'd.).
c) Coarse grain distribution.

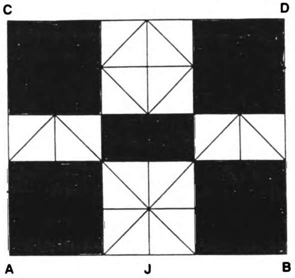

C

FIGURE 7 (cont'd.)

Figure 8. FEM input stress-strain curve of 'Alpha' and 'Beta' brasses.

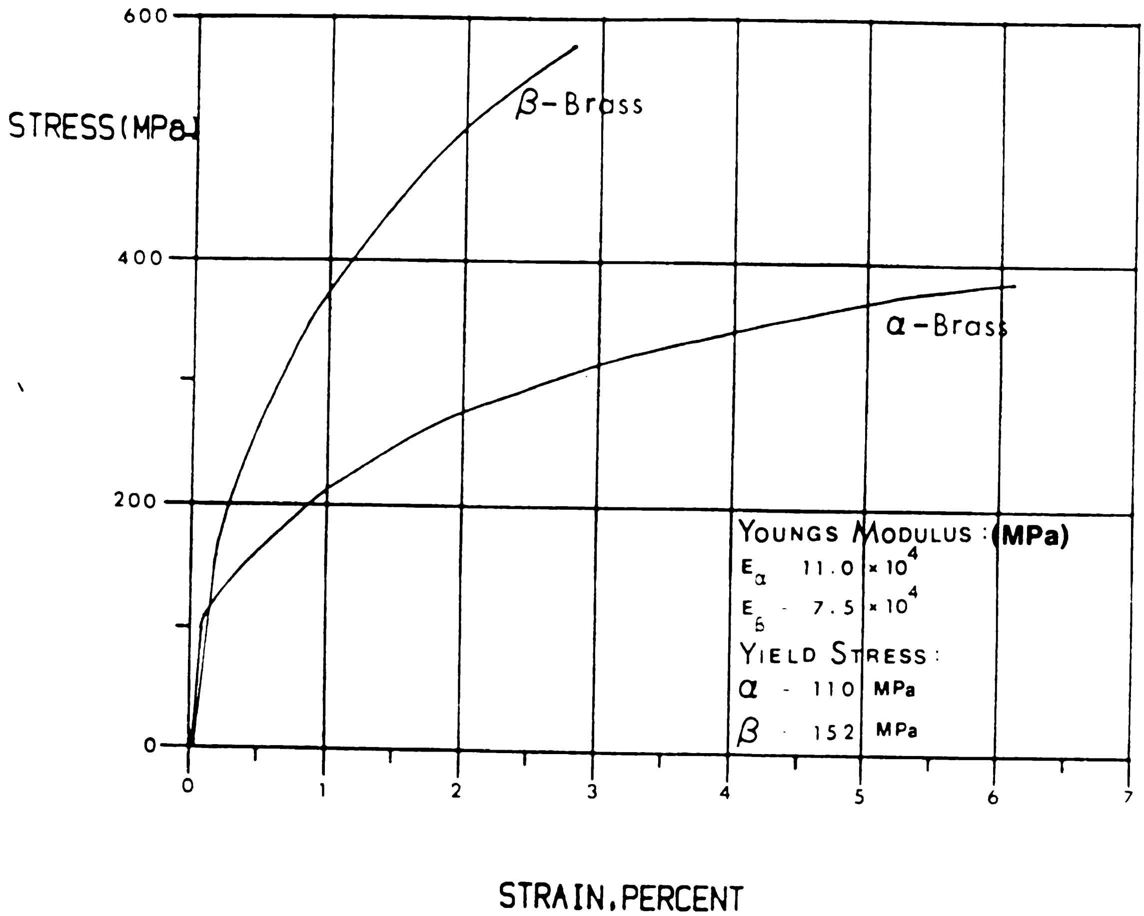
STRESS(MPa)
600
400
200
0
β-Brass
α-Brass
YOUNGS MODULUS : (MPa)
E_α 11.0 × 10^4
E_β - 7.5 × 10^4
YIELD STRESS :
α - 110 MPa
β - 152 MPa
0
1
2
3
4
5
6
7
STRAIN, PERCENT

FIGURE 8.

the common displacements of the nodes on the line $\overline{CD}$ and the initial length $\overline{AC}$, i.e. values of strain ϵ_y, corresponding to the prescribed values of stress σ_y were calculated as a weighted average of load displacements in the nodes along $\overline{CD}$ divided by $\overline{AC}$.

Stress-strain distribution plots were made by using meshes like the one presented in Figure 9. As mentioned earlier, all the beta particles in the mesh were incorporated into a single particle, keeping the volume fraction constant. Stresses on adjacent triangular elements, i.e. elements sharing a square in the mesh, were averaged to obtain stresses at the center of each square on line $\overline{GG}$. Strains were calculated from the displacements in the Y-direction of two successive nodes, one of which lies below the line $\overline{GG}$, and the other above the line $\overline{GG}$, shown in Figure 9. Accordingly, seven strain values and six stress values were calculated for each case.

Meshes in Figures 5, 6, and 7 could be considered to be a two-dimensional representation of a three-dimensional cylindrical test specimen. The meshes correspond to the upper half of the longitudinal section through the center of the specimen (51). Thus $\overline{AB}$ is the diameter of the tensile specimen and $\overline{CD}$ is the end of the upper half of the gauge length. It has been suggested that this two-dimensional representation can reasonably represent a three-dimensional behavior because the field equations in both cases have the same format (12). Stress-strain curves

Figure 9. FEM mesh, for alpha-beta brass containing 20 volume percent beta phase (shaded dark), used for calculation of the stress-strain distributions, across the alpha beta interface.

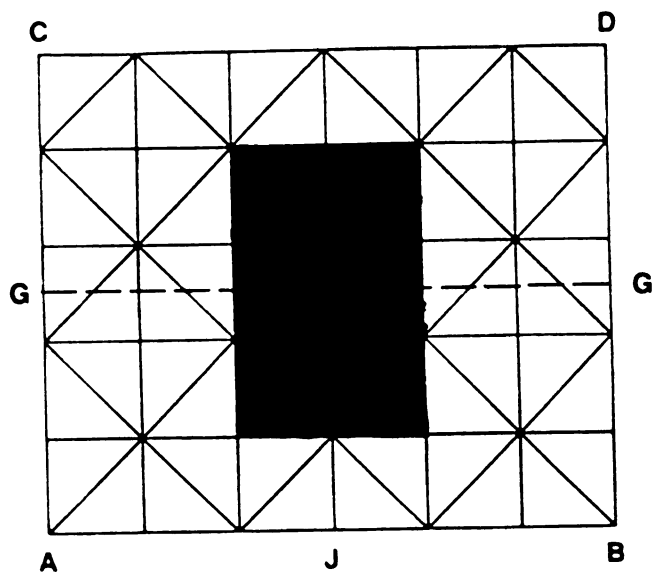

FIGURE 9.

were calculated by FEM for three cases, i.e. 20, 40 and 60 volume percent of beta phase. For each volume percent of beta phase, three different grain sizes were analyzed as shown in meshes in Figures 5, 6, and 7. Stress-strain distribution plots for the selected volume percents of beta phase and the three different grain sizes were also calculated. The detailed results of the FEM analysis are presented in the following chapter.

IV. RESULTS AND DISCUSSION

IV-A. TEM Analysis of the Deformation Structure in Alpha-Beta Brass

A detailed TEM analysis of the deformation structure in the two-phase alpha-beta brass could be divided into the following categories:

1) The analysis of the deformation structure in the alpha phase and the beta phase,
2) The deformation structure near the alpha-alpha and the beta-beta grain boundaries, and
3) The deformation structure near the alpha-beta phase boundary.

This study mainly focused on the analysis of the deformation structure in the alpha phase of the two-phase alpha-beta brass in the interior of the grain and near the alpha-alpha grain boundary. The results of this analysis are compared to prior investigations carried out on single phase 70Cu-30Zn alpha brass by Karashima (10,11) to check whether the deformation structure in the alpha phase of the two-phase alpha-beta brass is similar to the deformation structure in a single-phase alpha brass.

a) Overall Deformation Structure

General Observations: The polycrystalline specimens of 60Cu-40Zn brass were deformed to two different strain levels. The two strain levels chosen were 5 and 8 percents. The first part of this subsection discusses the deformation structure in specimens deformed to 5 percent strain level. The deformation structure in specimens strained to 8 percent strain level will be discussed in a later part of this subsection. In the second part of this subsection, observations relating to dislocation interaction with the boundary will be presented.

The deformation structure in the alpha phase, in specimens deformed to 5 percent strain level is presented in Figures 10, 11 and 12. It can be seen from Figures 10 and 11 that the dislocations in specimens deformed to 5 percent strain level were confined to definite single slip planes. No cross-slip was observed in specimens strained to this strain level. Dislocation tangling and complex dislocation structures were absent under these conditions. Another feature observed was pinning of the dislocations in some cases, as can be seen from Figure 12. With increased degree of deformation to 8 percent strain level dislocations present in two or three slip systems interacted an caused dislocation tangles. This resulted in complex dislocation structures such as those presented in Figures 13, 14 and 15. In specimens that were deformed to 8 percent strain, slip on intersecting slip planes was also observed.

Dislocation Interaction With the Boundary: Observation of the deformation structure in specimens that were deformed to 5 percent strain level presented in Figure 16(a), revealed dislocation pile-ups at the boundary. Absence of

Figure 10. Deformation Structure in the alpha phase of the alpha-beta brass deformed to 5 percent strain level.

FIGURE 10.

Figure 11. Deformation Structure in the alpha phase of the alpha-beta brass deformed to 5 percent strain level.

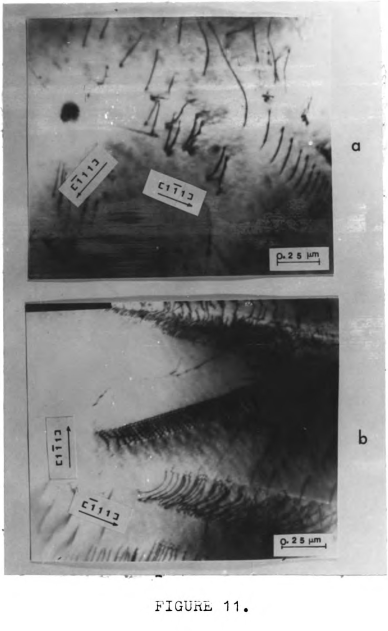

FIGURE 11.

Figure 12. Deformation Structure in the alpha phase of the alpha-beta brass deformed to 5 percent strain level.

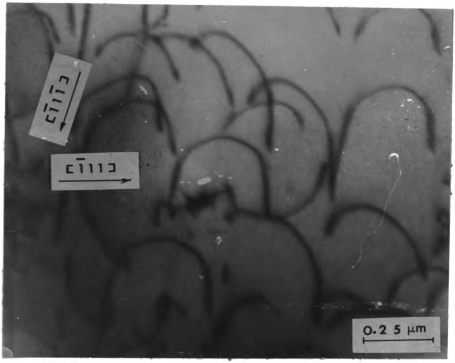

FIGURE 12.

Figure 13. Deformation Structure in the alpha phase of the alpha-beta brass deformed to 8 percent strain level.

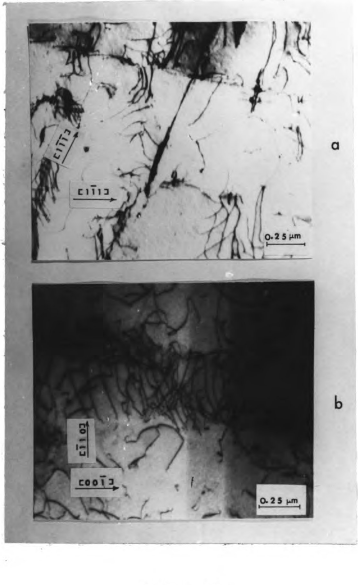

FIGURE 13.

Figure 14. Deformation Structure in the alpha phase of the alpha-beta brass deformed to 8 percent strain level.

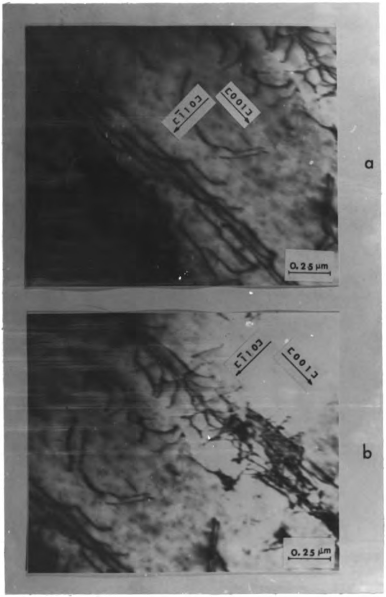

FIGURE 14.

Figure 15. Deformation Structure in the alpha phase of the alpha-beta brass deformed to 8 percent strain level.

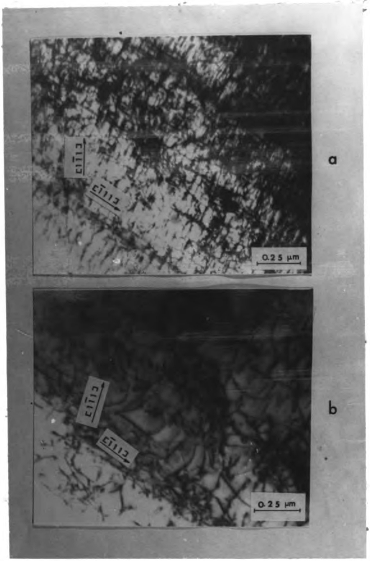

FIGURE 15.

progress of slip through the boundary suggested that this strain level was not sufficient enough to cause the dislocations to overcome the resistance to slip propagation provided by the boundary. However, in specimens that were deformed to 8 percent strain level dislocations piled-up at the boundary, initiated slip in the adjacent grain. This can be seen very clearly in Figure 16(b) and 16(c). Three models have been proposed to explain the initiation of deformation in the adjacent grain due to interaction of slip in one grain with the grain boundary. The stress concentration created due to the pile-up at the boundary either,

1) Forces the leading dislocations of the pile-up to move into the adjacent grain (39), or
2) Forces the boundary dislocation sources to multiply and cause dislocation motion into the adjacent grain (40), or
3) Activates some of the dislocation sources in the adjacent grain (41).

Slip nucleation at the grain boundary has been observed in Si-Fe, beta-Ti, Cu, Beta brass, alpha-Ti, Ni and 304 stainless steel (40). Margolin *et al.* (40) have studied grain boundary nucleation of slip in beta Ti- 8Mn alloy.

According to Nabarro (41), a slip band cannot cross from one grain to another without irregularity unless:

1) The slip direction is the same in both

Figure 16. Deformation structure in the alpha phase of the alpha beta brass near the boundary deformed to:

a) 5 percent strain level.

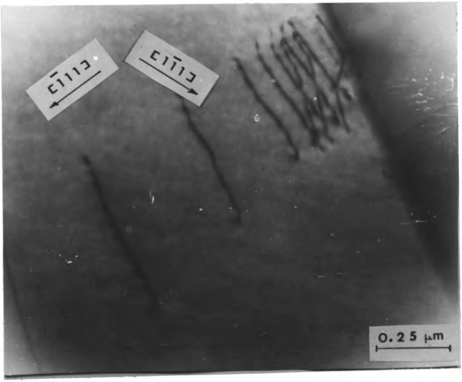

a

FIGURE 16.

Figure 16 (cont'd.).
b) and c) 8 percent strain level.

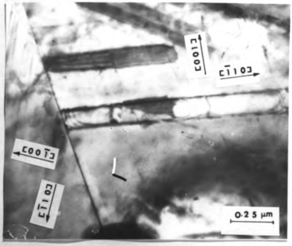

b

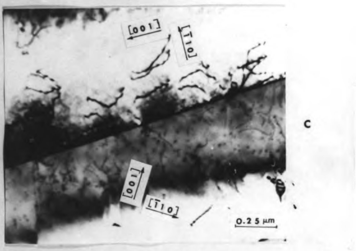

c

FIGURE 16 (cont'd.)

the grains, and

2) The choice of the crystal plane for slip is not critical in the adjoining grain.

According to Nabarro (41), when the slip directions are different in the adjacent grains, it is very difficult for a dislocation to pass from one grain into the adjacent grain as the stress needed to drive the dislocation through the grain would be of the order of the theoretical shear strength of the material. Hence, as a result of the difficulty in forcing a dislocation from one grain to another, Cottrell (41) suggested that, slip does not have to spread from one grain into the neighboring grain. Instead, the stress concentration created by the dislocation pile-up at the boundary may induce sources of dislocations, in the neighboring grains, to become active (41). In this case, the dislocations in the adjacent grain could be initiated from a source which is some distance away from the boundary. Such a feature can be observed in Figure 16(c), wherein the dislocations are seen to be present not very close to the boundary, but at a distance away from the boundary.

Karashima (10) has performed similar TEM analyses on 70Cu-30Zn alpha brass to study the deformation structure in this material. The results of his study can be summarized as follows:

1) In specimens that were strained from 1-5 percent dislocations were confined to slip planes, whereas

specimens that were strained from 5-10 percent revealed complex tangled dislocation structures.

2) Dislocation arrays piling up against the boundaries without slip propagation in the adjacent grain were observed at small strain (1-5 percent). On the other hand, continuation of slip across the boundaries was observed at higher strain levels (5-10 percent).

According to Karashima (10), the dislocation arrangements in a material, vary according to the degree of working. Thus, the work-hardening mechanisms during the various stages of deformation in turn are affected by the deformation structure in the material (10). The work-hardening, during the early stages of deformation, is mainly based upon the back stresses created due to the piling up of dislocations at the boundary (10). However, the formation of complex tangled dislocations and vacancy jogs is the main factor for the work-hardening in the later stages of deformation. Formation of such complex sessile dislocations is a prominent characteristic observed during deformation of alpha brass. However, in materials with a high stacking fault energy like beta brass or aluminum (10), most of the dislocations introduced during cold-working are confined to single slip planes, and thus formation of complex tangled dislocation structure is not a very common feature in such materials.

On comparing the results of the present study with the investigations on single phase 70Cu-30Zn alpha brass by Karashima (10), one can notice a close similarity between the deformation behavior in the alpha phase of the two-phase alpha-beta brass and the single phase alpha brass.

b) <u>Burgers Vector Analysis of Dislocations near the Boundary</u>

Burgers vector analysis of dislocations near the boundary was performed to determine the character of dislocations in their relaxed configuration. The analysis also provides details of the active slip plane and the active slip direction. A set of dislocations in the alpha phase near a boundary with different diffraction vectors are presented in Figure 17. There are two types of dislocations in this set, marked as 'A' and 'B'. Burgers vector analysis of the dislocations showed that both types of dislocations 'A' and 'B' were of mixed character. Dislocations of type 'A' have a Burgers vector of $a/2[1\bar{1}0]$ and that of type 'B' have a Burgers vector of $a/2[01\bar{1}]$. The results of this analysis are tabulated in Table 5. Another set of dislocations present in the alpha phase near a boundary with different diffraction vectors is presented in Figure 18. This set of dislocations, also has two types of dislocations marked as 'C' and 'D'. Burgers vector analysis showed that the dislocations of type 'C' are mixed in nature, whereas that of type 'D' are screw in nature. The Burgers vector of dislocations of type 'C' is $a/2[1\bar{1}0]$,

Figure 17. Dislocations near the boundary in the alpha phase of the alpha-beta brass with different diffraction vectors:

a) $\vec{g} = [\bar{1}11]$

b) $\vec{g} = [002]$

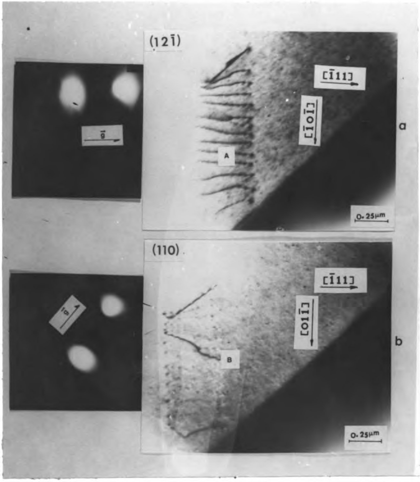

(12$\bar{1}$)
[$\bar{1}$11]
[$\bar{1}$0$\bar{1}$]
g
A
0.25µm
a
(110)
[$\bar{1}$11]
[01$\bar{1}$]
g
B
0.25µm
b

FIGURE 17.

Figure 17 (cont'd.).
c) $\bar{g} = [20\bar{2}]$
d) $\bar{g} = [11\bar{1}]$

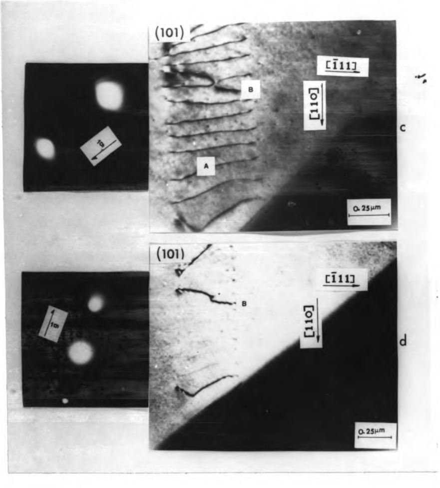

FIGURE 17 (cont'd.)

TABLE 5

Results of the Burgers Vector
Analysis of Dislocations in Figure 17.

Type of Dislocations	Burgers Vector	Slip Plane	Direction	Character
A	$[1\bar{1}0]$	(111)	$[2\bar{1}\bar{1}]$	Mixed
B	$[01\bar{1}]$	(111)	$[\bar{1}10]$	Mixed

Figure 18. Dislocations near the boundary in the alpha phase of the alpha-beta brass with different diffraction vectors:

a) $\vec{g} = [\bar{1}11]$

b) $\vec{g} = [002]$

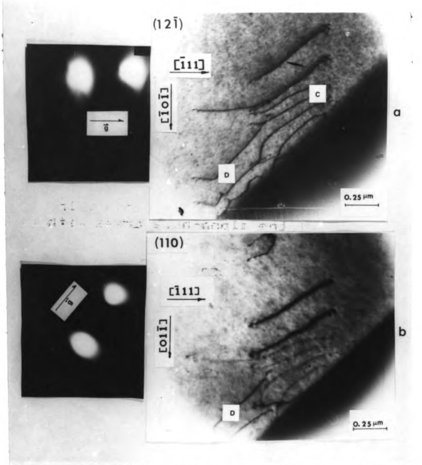
(12$\bar{1}$)
[$\bar{1}$11]
[$\bar{1}$0$\bar{1}$]
g
C
D
a
0.25 μm
(110)
[$\bar{1}$11]
[01$\bar{1}$]
g
D
b
0.25 μm

FIGURE 18.

Figure 18 (cont'd.).
c) $\vec{g} = [20\bar{2}]$
d) $\vec{g} = [020]$

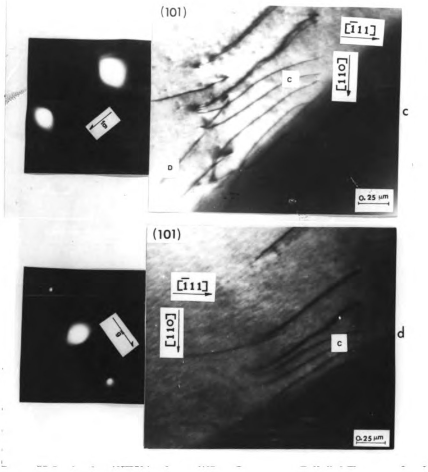

FIGURE 18 (cont'd.)

TABLE 6

Results of the Burgers Vector Analysis of Dislocations in Figure 18.

Type of Dislocations	Burgers Vector	Slip Plane	Direction	Character
C	[1$\bar{1}$0]	(111)	[10$\bar{1}$]	Mixed
D	[10$\bar{1}$]	(111)	[10$\bar{1}$]	Screw

whereas that of type 'D' is a/2[10$\bar{1}$]. The results of this analysis are tabulated in Table 6.

Another set of dislocations in the alpha phase near a boundary are seen in Figure 19. Dislocations that occur as pairs (henceforth referred to as "Dislocation-Pairs") are clearly visible in these figures. These pairs are indicated by arrows. Dislocations in this set, as marked as 'E', are screw in nature with a Burgers vector of a/2[10$\bar{1}$]. Table 7 gives the details of the Burgers vector analysis of these dislocations. The "Dislocation-Pairs" observed in Figure 19 are discussed in more detail in the following subsection. All the specimens used for the Burgers vector analysis were deformed to a 5 percent strain level.

c) <u>Analysis of "Dislocation-Pairs"</u>

An important observation made during the TEM analysis was the presence of "Dislocation-Pairs" in the alpha phase of the alpha-beta brass. These "Dislocation-Pairs" were observed to occur successively on a slip plane.

Karashima (11) in his investigations on alpha brass observed similar dislocation pairs in deformed alpha brass. He discounted the possibility that they could be double-images of dislocations produced due to the TEM contrast effects. His analysis is based on the observation that some of the dislocations produce single dislocation images, whereas their neighbors possessing the same

Figure 19. Dislocations near the boundary in the alpha phase of the alpha-beta brass with different diffraction vectors:

a) $\vec{g} = [\bar{1}11]$

b) $\vec{g} = [002]$

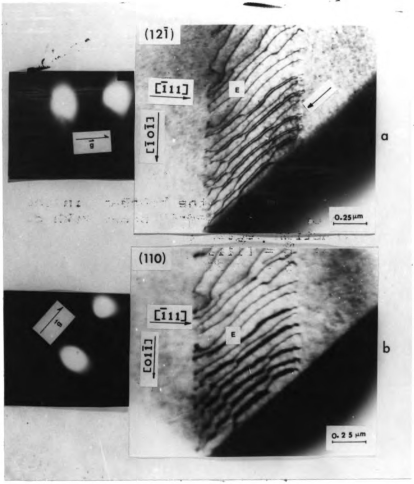
(12$\bar{1}$)
[$\bar{1}$11]
[$\bar{1}$0$\bar{1}$]
E
a
0.25 μm
(110)
[$\bar{1}$11]
[01$\bar{1}$]
E
b
0.25 μm

FIGURE 19.

Figure 19 (cont'd.).

c) $\vec{g} = [20\bar{2}]$

d) $\vec{g} = [11\bar{1}]$

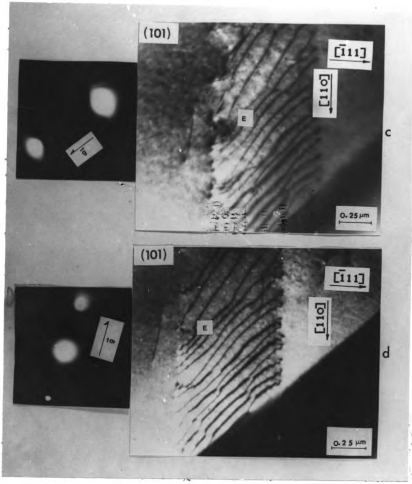

FIGURE 19 (cont'd.)

TABLE 7

<u>Results of the Burgers Vector Analysis of Dislocations in Figure 19.</u>

Type of Dislocations	Burgers Vector	Slip Plane	Direction	Character
E	$[10\bar{1}]$	(111)	$[10\bar{1}]$	Screw

character appear as "double images". Such an observation cannot be explained on the basis of TEM contrast effects. Karashima (11) has considered two possibilities to explain the occurance of these "Dislocation-Pairs". One suggestion is that these pairs are superlattice dislocations, however, as he has pointed out, presence of superlattice dislocations or long-range order has not been reported in alpha brass (11). On this basis, the double images of dislocations observed in the alpha phase of the alpha-beta brass cannot be due to superlattice formation. Another suggestion by Karashima is that these are unit dislocations moving in pairs; the second one pushing the first in order to overcome short-range order hardening. Seeger (61) has originally proposed such a theory for Ag-Au binary alloys. Karashima considered this hypothesis to be a possible explanation for explaining the occurrence of "Dislocation-Pairs" because short-range order hardening has been reported in alpha brass (11). In the present investigation, Burgers vector analysis was performed on such paired dislocations observed in Figure 19. This analysis showed that these "Dislocation-Pairs" possessed screw character. So they may be dislocations that have cross-slipped onto parallel slip planes due to dislocation pile-up stresses that arise at the boundary region. The results of the Burgers vector analysis performed on such "Dislocation-Pairs" are tabulated Table 7 (refer to the previous subsection). It can be observed from Figure 19 that the dislocations occur in pairs only near a boundary,

whereas, the dislocations present in the same slip plane at a distance away from the boundary are single. Based on this observation, the formation of "double-images" could be explained in the following manner. As dislocations approach a boundary, their movement is inhibited by the back stresses created due to dislocation pile-up at the boundary. To overcome this resistance created due to the pile-up of dislocations, the screw dislocations double cross-slip onto parallel slip planes. In the relaxed state they will arrange themselves into a minimum energy configuration (62). These cross-slipped screw dislocations will appear as pairs when observed in the TEM under certain tilt conditions. The above mentioned hypothesis could also explain why these dislocations occur in pairs only near the boundary, and not away from it. At locations away from the boundary, the dislocations do not have to cross-slip due to the absence of the pile-up stresses. Hingwe *et al.* (2) and Nilsen *et al.* (4) have observed similar cross-slipping phenomena in the alpha phase of bicrystals of alpha-beta brass. Optical and Scanning Electron Microscopy analysis performed during their investigations revealed that slip lines in the alpha phase, when approaching the alpha-beta phase boundary result in cross-slip or multiple-slip to avoid crossing the phase boundary. Subramanian (62) has proposed that screw dislocations, after cross-slipping onto parallel planes, arrange themselves in a minimum energy configuration in the relaxed state. The "Dislocation-Pairs" have also been observed to occur in random fashion among tangled dislocations as can be seen in Figure 20 (indicated by arrows).

The hypothesis that these dislocation pairs are screw dislocations that have cross-slipped onto parallel planes could also explain the occurence of these pairs among tangled dislocations, because tangled sessile dislocations hinder the motion of dislocations in a fashion similar to the resistance offered to the dislocation movement by grain boundaries. Further studies need to be performed to clarify this proposed model for the occurence of such "Dislocation-Pairs".

d) Grain Boundary Dislocations

The boundary dislocations observed in the specimens of alpha-beta brass are seen in Figures 21 and 22. These dislocations, as can be noted from the figure are not dislocations in a slip trace, but are present in a boundary. Close examination of diffraction patterns on both sides of the boundary, revealed a slight angular rotation between the diffraction patterns, indicating that these dislocations are present in a low-angle tilt boundary.

e) In-Situ Deformation Studies in a High Voltage Electron Microscope (HVEM)

Apart from TEM studies of the deformation structure in a conventional 100KV Electron Microscope, preliminary investigations of *in-situ* deformation of micro-tensile

Figure 20. "Dislocation-Pairs" observed in the alpha phase of the alpha-beta brass.

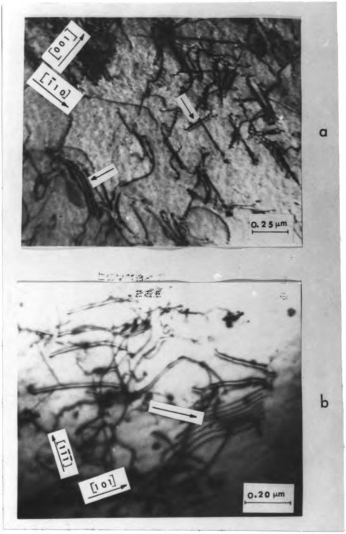

FIGURE 20.

Figure 21. Boundary dislocations observed in the alpha phase of the alpha-beta brass.

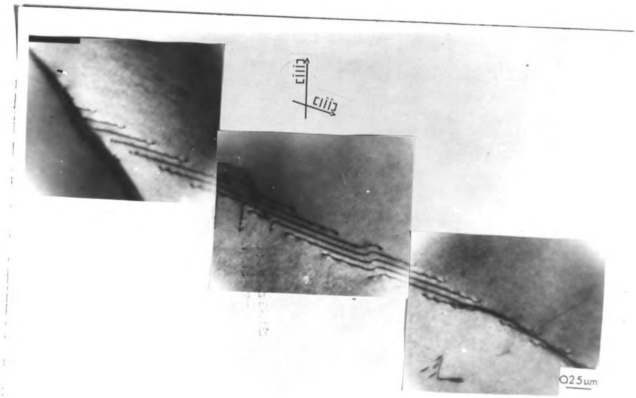

FIGURE 21.

Figure 22. Boundary dislocations observed in the alpha phase of the alpha-beta brass.

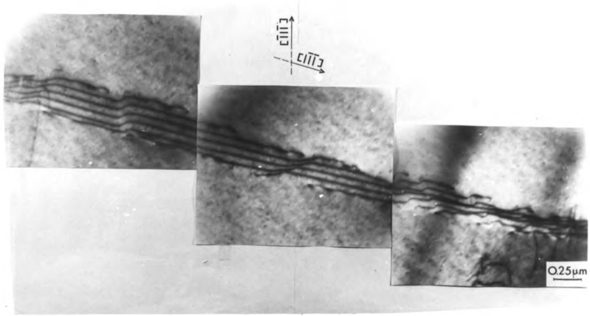

FIGURE 22.

specimen of alpha-beta brass in an HVEM were carried out. Figures 23 and 24 are those of dislocations that were in motion during *in-situ* deformation in an HVEM. These still photographs were taken from a video-tape on which the dislocation motion was recorded. Dislocations moving in a slip trace are seen in Figure 23 (marked as 'F' on the photograph). Dislocation pile-ups (marked as 'G') and dislocations moving on intersecting slip planes (marked as 'H') during *in-situ* deformation in an HVEM are presented in Figure 24.

IV-B. FEM Analysis of Stress-Strain Behavior of Alpha-Beta Brass

The results of the present FEM analysis could be divided into the following categories:

1) Analysis of the stress-strain relationships for different volume percents of beta phase,

2) Analysis of the stress-strain relationships for different grain sizes of alpha-beta phases,

3) Analysis of the stress-strain distributions across the alpha-beta interface, and

4) Comparison of experimental and FEM calculated stress-strain curves.

a) Stress-strain Relationships for Different Volume Percents of Beta Phase

FEM calculated stress-strain curves of alpha-beta brass for three different volume percentages of beta phase (20, 40 and 60) are illustrated in Figure 25. As can be observed

Figure 23. Still photographs of dislocations in motion in the alpha phase of the alpha-beta brass during *in-situ* deformation in an HVEM.

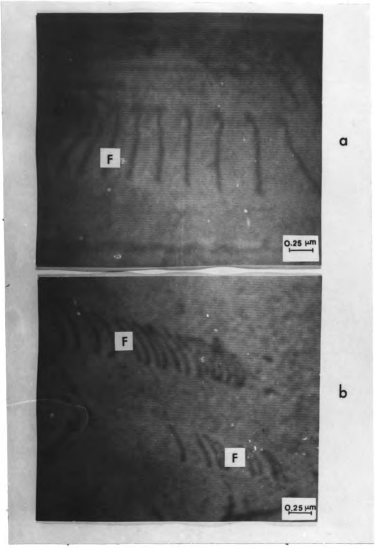

FIGURE 23.

Figure 24. Still photographs of dislocations in motion in the alpha phase of the alpha-beta brass during *in-situ* deformation in an HVEM.

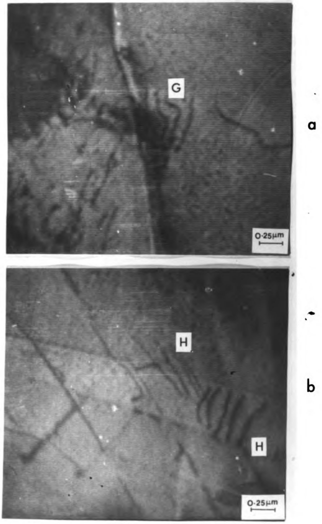

FIGURE 24.

from this figure the stress-strain curve for 60 volume percent beta phase attains higher stress levels for similar strain levels, as compared to the stress-strain curve for 40 volume percent beta phase (in the plastic region). Similarly, the stress-strain curve for 40 volume percent beta phase, in turn, reaches higher stress levels for a given strain level, when compared to the stress-strain curve for 20 volume percent beta phase (in the plastic region). The grain sizes and the phase distributions of beta phase used in the meshes for the calculation of these stress-strain curves are shown in Figures 5(a), 6(a) and 7(a). As can be observed, all three curves deviate from linearity at a stress level of about 110-150 MPa. Although the exact yield stress level of each curve is difficult to determine, an approximate estimate of the value could be obtained by using the 0.2 percent offset method for Yield point determination. The yield stress values from the three stress-strain curves, obtained by using the "Offset Method" are tabulated in Table 8. These values compare very well with the published handbook values of yield stress for alpha-beta brass (refer to Table 1).

b) Stress-Strain Relationships for Different Grain Size Distributions

Stress-strain curves of alpha-beta brass containing 20, 40 and 60 volume percent of beta phase, for different grain sizes were calculated by using FEM analysis. The stress-strain curves of alpha-beta brass containing 20

Figure 25. FEM calculated curves of alpha-beta brass for 20, 40 and 60 volume percents of beta phase.

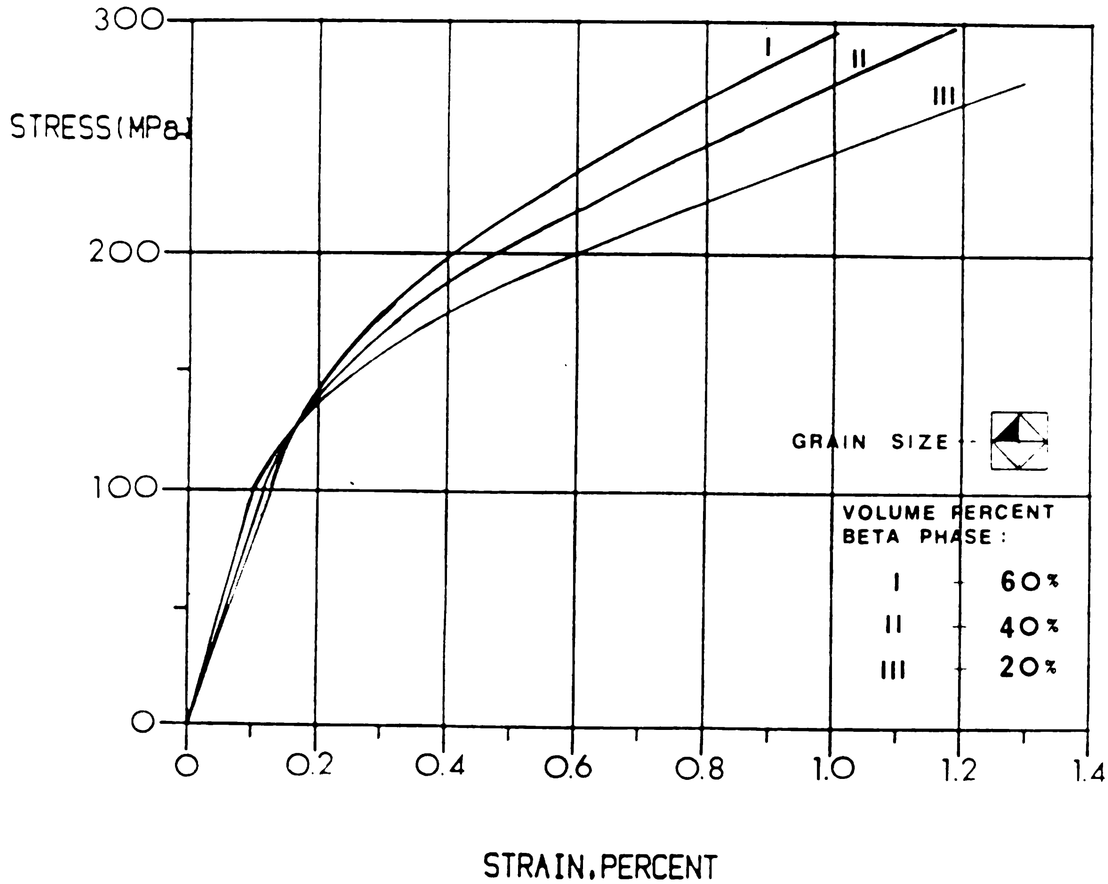

300
200
100
0
STRESS(MPa)
I
II
III
GRAIN SIZE
VOLUME PERCENT
BETA PHASE :
I - 60%
II - 40%
III - 20%
0
0.2
0.4
0.6
0.8
1.0
1.2
1.4
STRAIN, PERCENT

FIGURE 25.

TABLE 8

Yield Stress Values Obtained by Using the 0.2 Percent Offset Method from Curves in Figure 25.

Curve	Volume Percent Beta Phase	Yield Stress (MPa)
I	20	160
II	40	175
III	60	210

volume percent beta phase for two different grain sizes are presented in Figure 26. It can be seen from the figure that as the grain size gets smaller, the stress-strain curve tends to shift upwards, i.e. for equal strain levels, the stress-strain curve for finer grain size attains higher stress levels than the stress-strain curve for a coarser grain size (in the plastic region). The stress-strain curves at two different grain sizes for alpha-beta brass containing 40 volume percent of beta phase, are presented in Figure 27, and the stress-strain curves at two different grain sizes for alpha-beta brass containing 60 volume percent beta phase are presented in Figure 28. In both these figures, it can be observed that the stress-strain curve for a finer grain size reaches higher stress levels (for a given strain) than the stress-strain curve for a coarser grain size (in the plastic range). One possible explanation for this behavior according to Jinoch *et al.* (12) is that the flow stress, at a given strain level, for a finer particle configuration is higher than for a coarse particle configuration. This is because the strain difference between the alpha and the beta phases is smaller for a finer particle configuration (12). When the particle configuration is coarse, the strain in the softer alpha phase is much greater than the strain in the harder beta phase. Whereas, when the particle configuration is finer, the difference in strain levels between the alpha and the beta phases is not so large. Hence, as a result, the

Figure 26. FEM calculated stress-strain curves of alpha-beta brass containing 20 volume percent beta phase for fine (I) and coarse (II) grain size distribution.

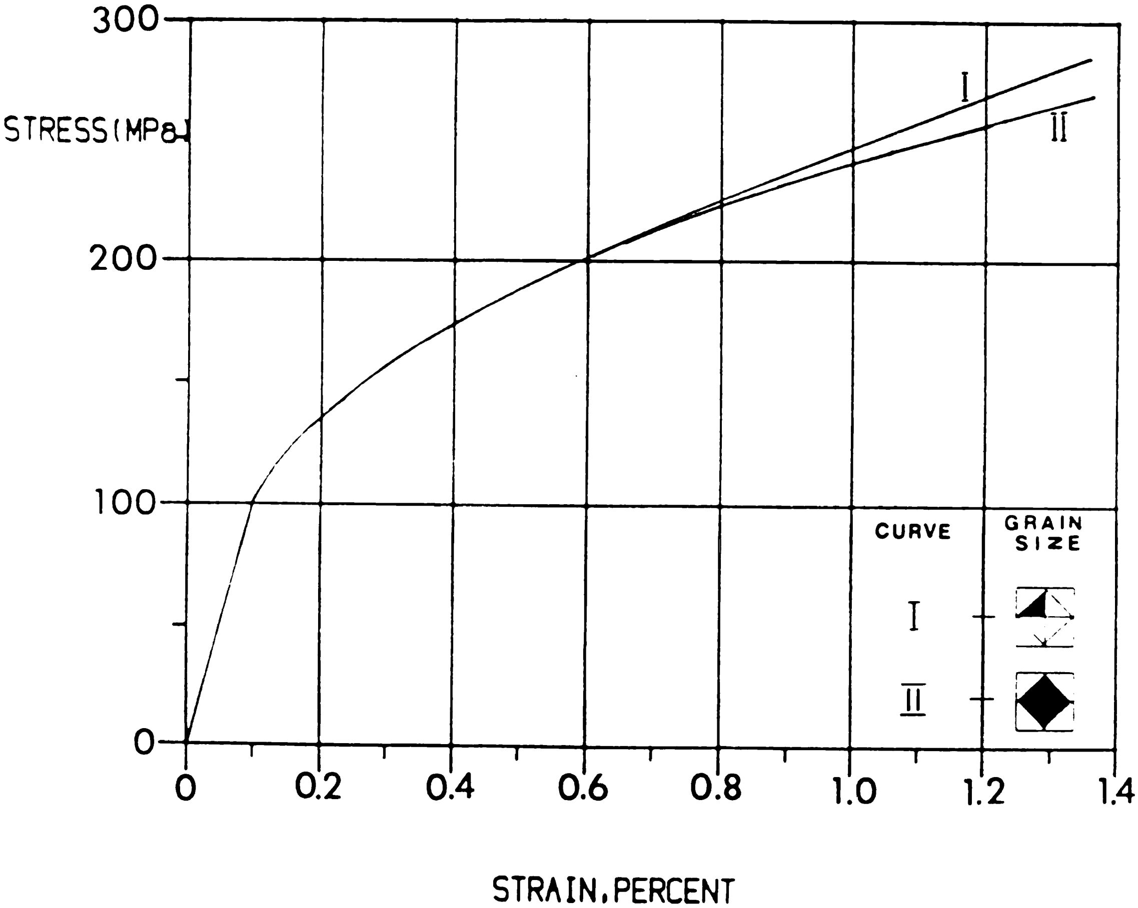
300
STRESS(MPa)
200
100
0
0
0.2
0.4
0.6
0.8
1.0
1.2
1.4
I
II
CURVE
GRAIN SIZE
I
II
STRAIN, PERCENT

FIGURE 26.

Figure 27. FEM calculated stress-strain curves of alpha-beta brass containing 40 volume percent beta phase for fine (I) and coarse (II) grain size distribution.

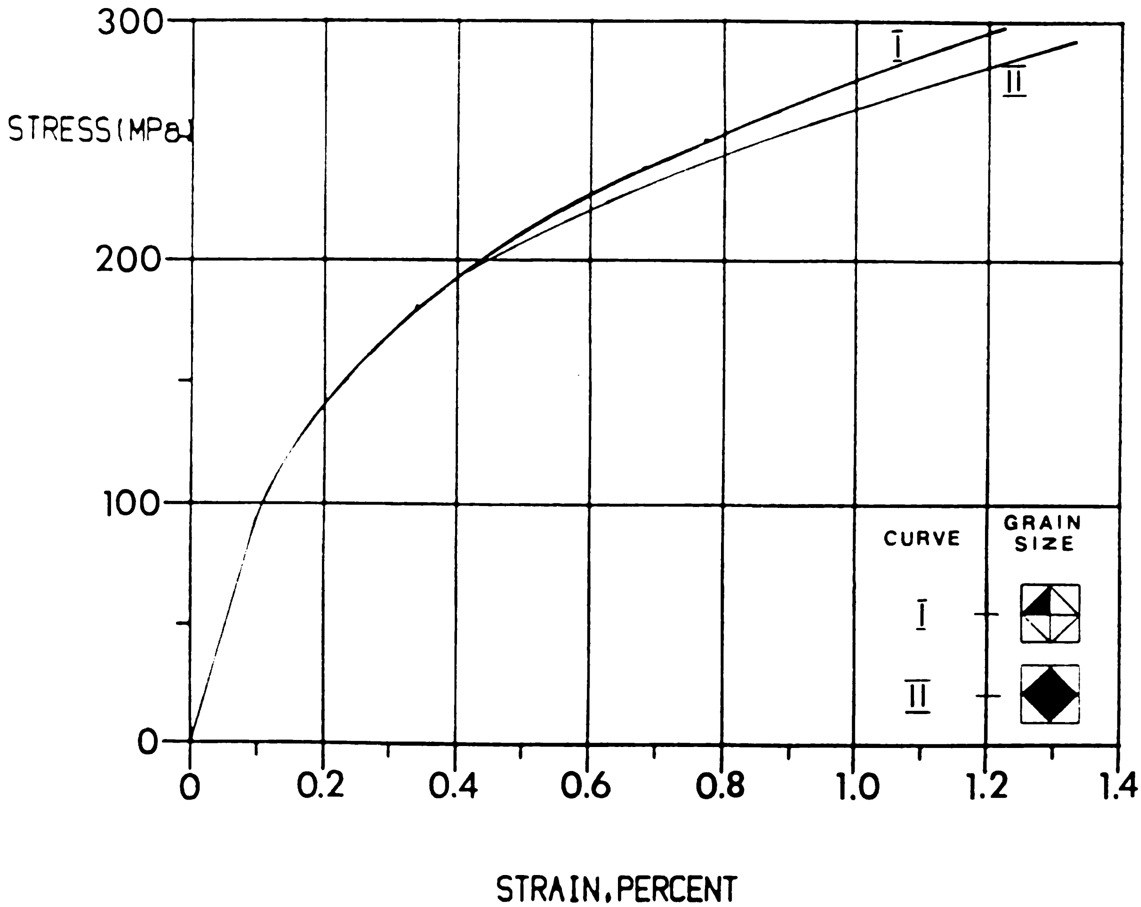

300
200
100
0
STRESS(MPa)
I
II
CURVE
GRAIN SIZE
I
II
0
0.2
0.4
0.6
0.8
1.0
1.2
1.4
STRAIN, PERCENT

FIGURE 27.

Figure 28. FEM calculated stress-strain curves of alpha-beta brass containing 60 volume percent beta phase for fine (I) and coarse (II) grain size distribution.

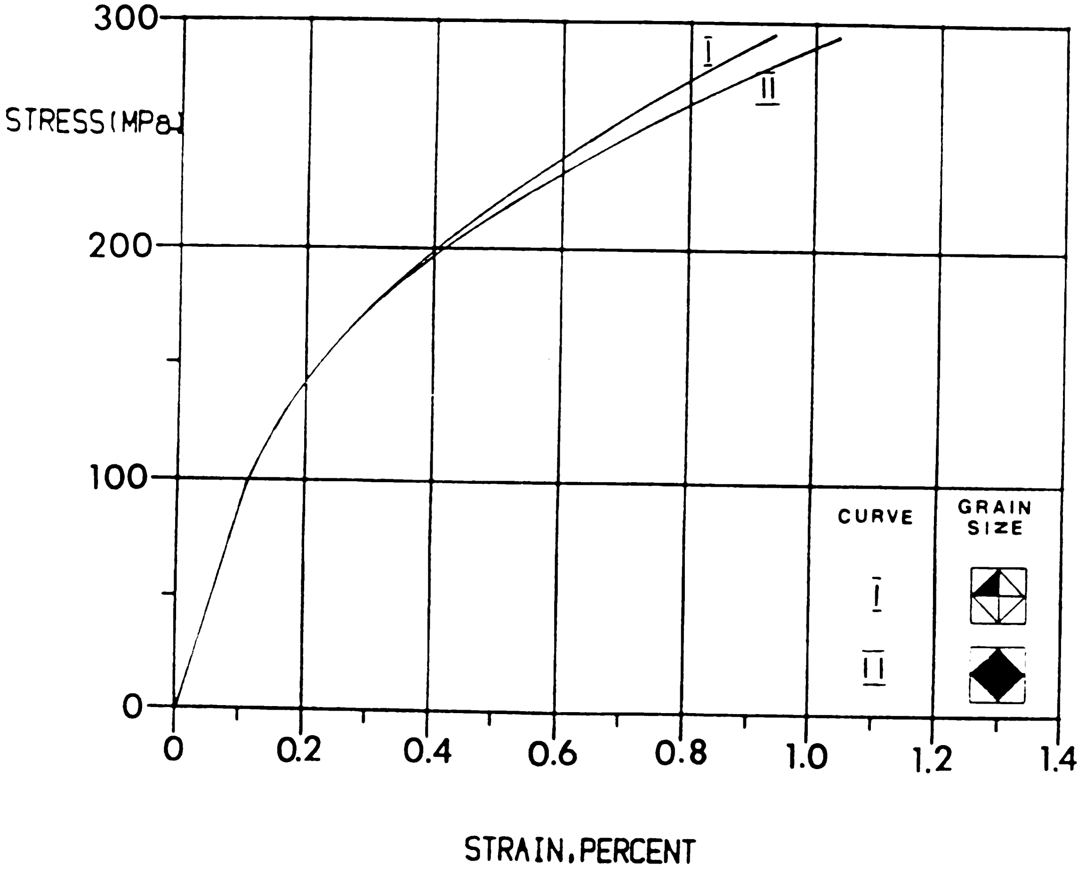
300
200
100
0
STRESS(MPa)
0
0.2
0.4
0.6
0.8
1.0
1.2
1.4
STRAIN, PERCENT
I
II
CURVE
GRAIN SIZE
I
II

FIGURE 28.

stiffer beta phase undergoes considerably larger strain. Since the beta phase is stiffer, larger strains in beta induce the stress levels to reach a higher value. This,in turn, results in the stress-strain curve for a finer particle configuration to reach higher stress levels (51) than the curve for a coarser particle configuration. The relative grain sizes and the phase distributions used in the meshes to calculate the stress-strain curves are presented in Figures 5, 6 and 7.

c) Stress-Strain Distributions Across the Alpha-Beta Interface

Stress distributions in the alpha-beta brass containing 20 volume percent beta phase, in each element across the line $\overline{GG}$ in Figure 9, are plotted in Figures 29 and 30. The stress distributions across the phases are calculated in the loading Y-direction and in the transverse X-direction. The stress distributions have been calculated for three different externally applied stress levels, i.e. 207, 241 and 276 MPa for distributions in the Y-direction, and 172, 207 and 241 MPa, for distributions in the X-direction. Large differences in the stress levels in both the X- and Y-directions are evident from Figure 29 and 30. For stress distributions in the loading Y-direction, the stresses in the beta phase were found to be considerably higher than the stresses in the alpha phase, as can be observed in Figure 29, for any particular level of externally applied stress. Stress distribution in the

Figure 29. FEM calculated stress distribution plot for alpha-beta brass contaiing 20 volume percent beta phase, in the loading Y-direction.

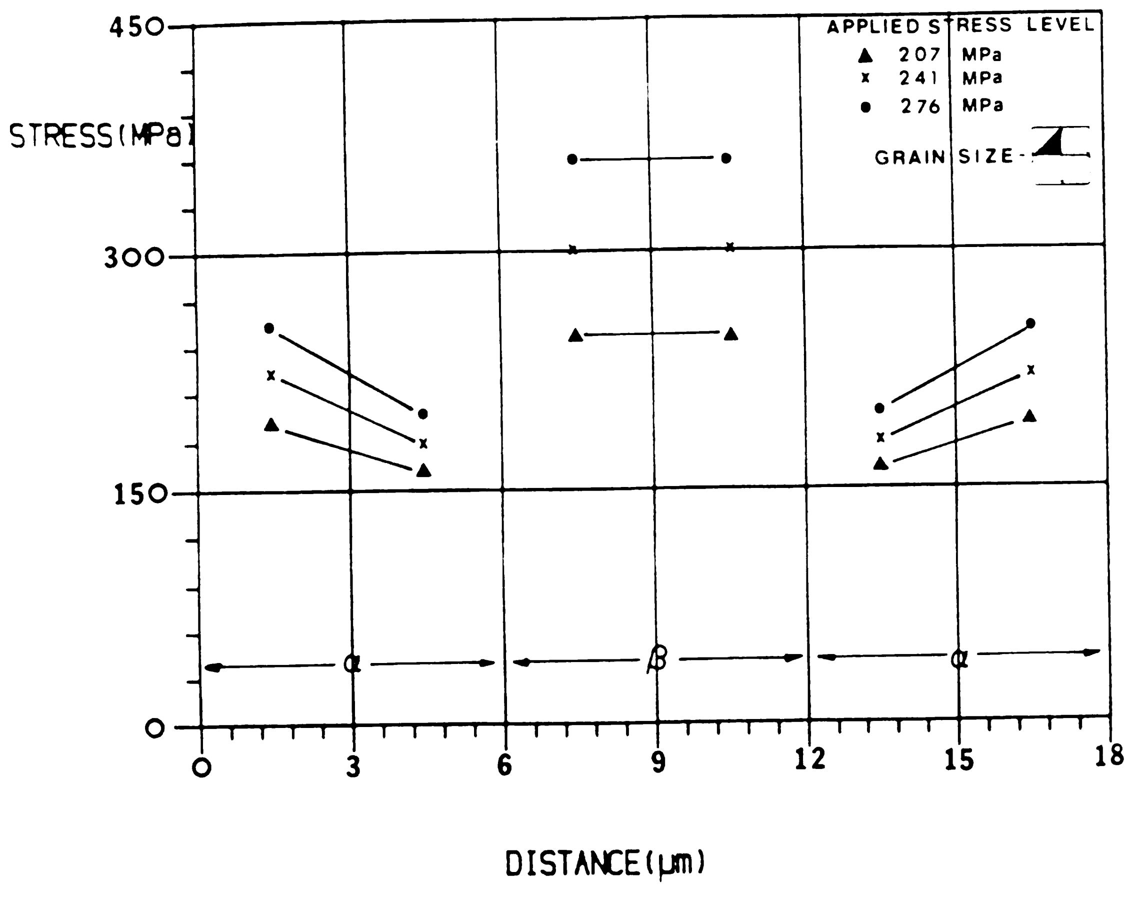

APPLIED STRESS LEVEL
207 MPa
241 MPa
276 MPa
GRAIN SIZE
STRESS(MPa)
450
300
150
0
α
β
α
0
3
6
9
12
15
18
DISTANCE(μm)

FIGURE 29.

Figure 30. FEM calculated stress distribution plot for alpha-beta brass containing 20 volume percent beta phase, in the transverse X-direction.

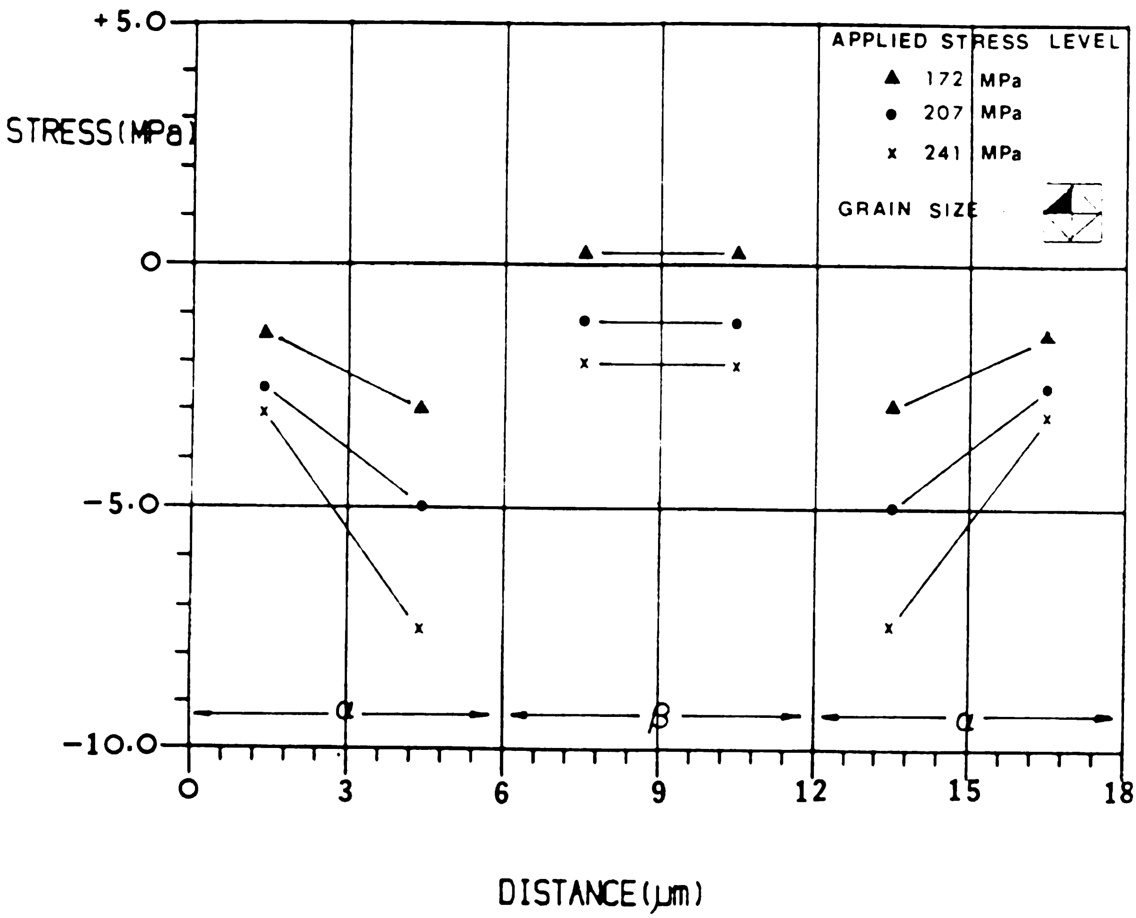

+5.0
0
-5.0
-10.0
STRESS(MPa)
APPLIED STRESS LEVEL
172 MPa
207 MPa
241 MPa
GRAIN SIZE
α
β
α
0
3
6
9
12
15
18
DISTANCE(μm)

FIGURE 30.

transverse X-directions also showed steep gradients across the phases. Stresses were found to be generally compressive in nature in the transverse X-direction at the applied stress levels, as can be observed in Figure 30. The difference in the stress levels between the alpha and the beta phase tended to increase at higher externally applied stress levels. At stress levels of 172 MPa and below, the stresses in the transverse X-direction in the beta phase, were found to be tensile in nature, whereas the stresses in the alpha phase were compressive.

This is probably due to a lower Young's modulus value of the beta phase as compared to the alpha phase. As a result of this, beta phase expands more along the Y-direction as compared to the alpha phase. This in turn will require the beta phase to contract more in the X-direction. The alpha phase resists this and may cause tensile stresses in the beta phase. At higher stress levels, the beta phase undergoes plastic deformation and experiences compression like the alpha phase.

The stress contour distributions in the 60 element mesh used for the FEM analysis are presented in Figure 31 and 32. The stress levels at different locations on the mesh are marked. The stress contour distribution for stresses in the loading Y-direction at an externally applied stress level of 207 MPa is presented in Figure 31. The stress contour distribution for stresses in the transverse X-direction at the same external stress level is

Figure 31. FEM generated stress contour distribution plot in the 60 element mesh for alpha-beta brass containing 20 volume percent beta phase, in the loading Y-direction. (The stress levels marked are in MPa).

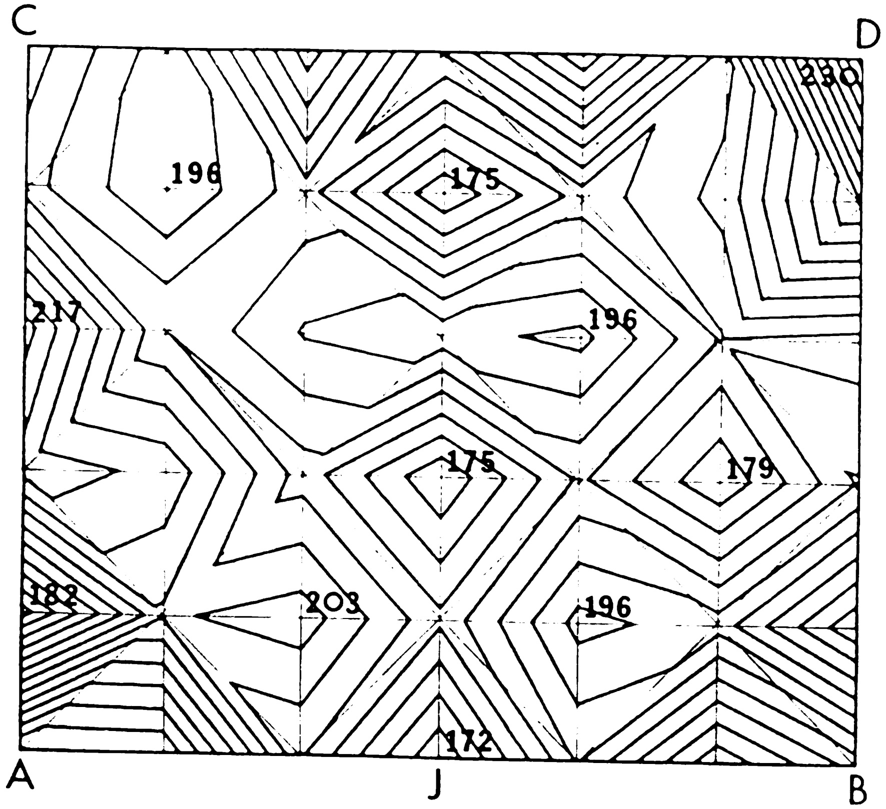

FIGURE 31.

Figure 32. FEM generated stress contour distribution plot in the 60 element mesh for alpha-beta brass containing 20 volume percent beta phase, in the transverse X-direction. (The stress levels marked are in MPa).

Figure 33. FEM calculated strain distribution plot for alpha-beta brass containing 20 volume percent beta phase.

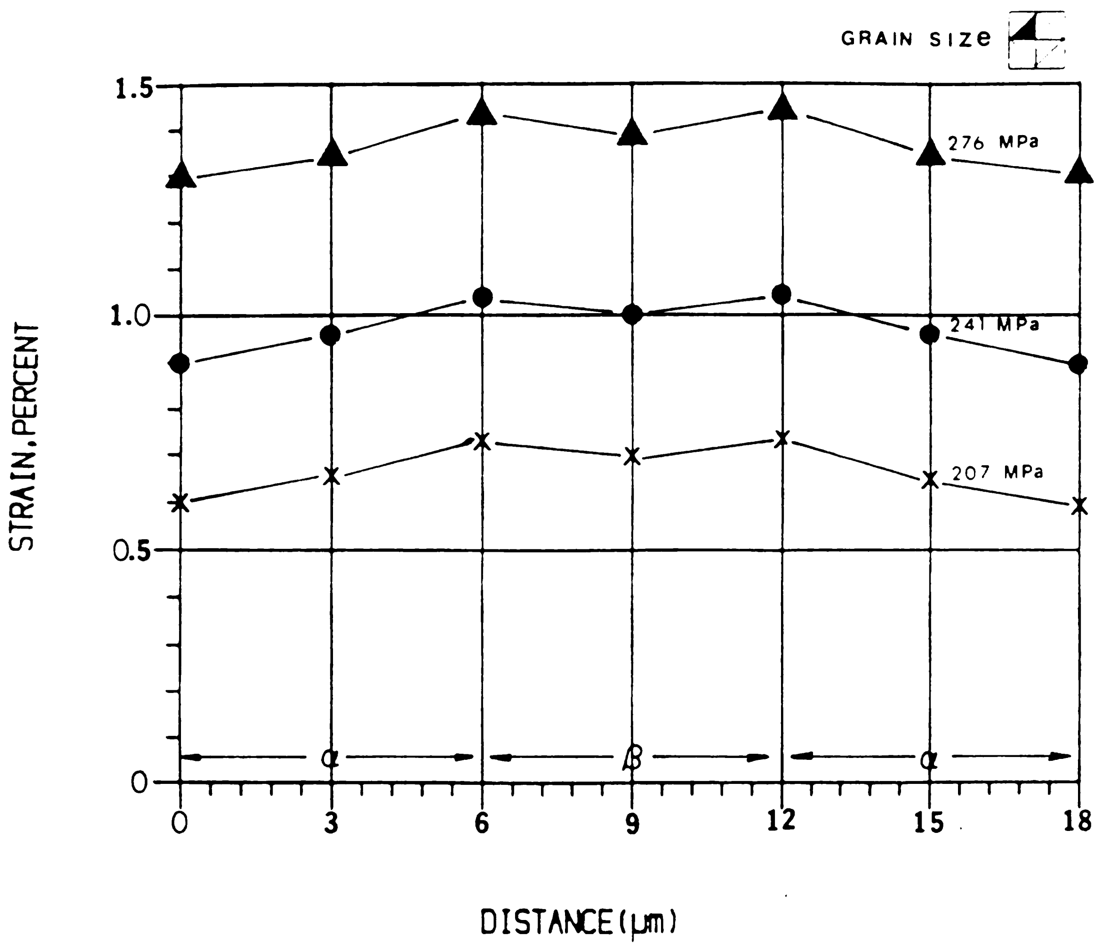
GRAIN SIZE
1.5
1.0
0.5
0
276 MPa
241 MPa
207 MPa
α
β
α
0
3
6
9
12
15
18
STRAIN, PERCENT
DISTANCE(μm)

FIGURE 33.

presented in Figure 32. The stress contour distributions shown in Figures 31 and 32 are plotted for alpha-beta brass containing 20 volume percent beta phase for the grain size and phase distributions shown in Figure 5(a).

The strain distributions across the phases on line $\overline{GG}$ (see Figure 9) is plotted in Figure 33. As can be observed from this figure, the strains in the beta phase were generally higher than the strains in alpha phase at the externally applied stress levels. Strains in the beta phase were higher near the alpha-beta interface as compared to the strains in the beta grain interior. The strain gradients calculated in this analysis, however, were not as steep as those observed by Jinoch *et al.* (12) in their FEM investigations of Ti- 8Mn alloy. This difference in the steepness of the strain gradients may be due to the larger difference in the yield stress values of the alpha and beta Ti- 8Mn input curves, as compared to the difference in the yield stress values of the alpha and beta brass input curves used during the present FEM analysis.

d) Comparison of Experimental Stress-Strain Curve with the FEM Calculated Curves

A comparison of the FEM calculated stress-strain curve of alpha-beta brass (containing 20 volume percent beta phase; same as in the 60Cu-40Zn brass) with the experimental one is made in Figure 34. As can be seen from the figure, the FEM calculated stress-strain curve is at a higher level than the experimental curve. One possible

Figure 34. Comparison between the experimentally determined stress-strain curve of 60Cu-40Zn brass and the FEM calculated curve of alpha-beta brass containing 20 volume percent beta phase.

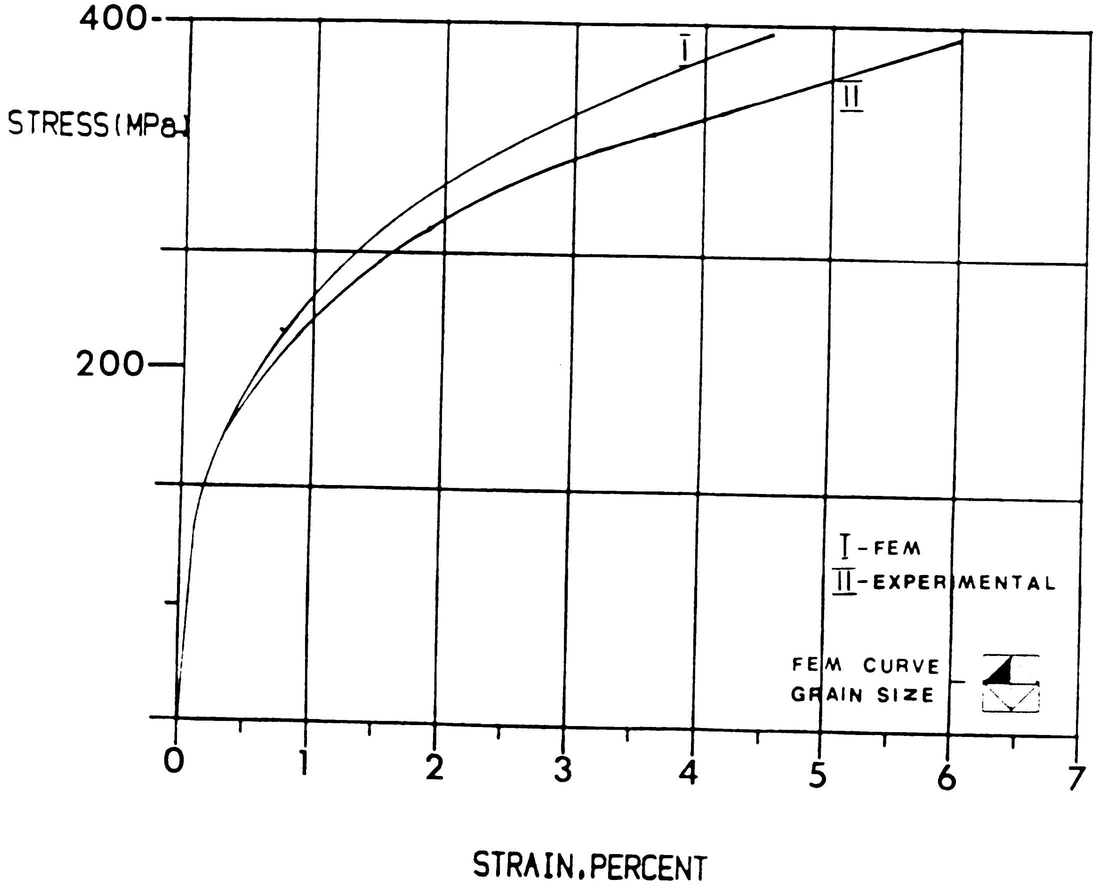

400
STRESS(MPa)
200
I
II
I-FEM
II-EXPERIMENTAL
FEM CURVE
GRAIN SIZE
0
1
2
3
4
5
6
7
STRAIN, PERCENT

FIGURE 34.

explanation is the following: The FEM input curve for the alpha brass used during the analysis was extrapolated by performing a tensile test on a 70Cu-30Zn tensile specimen and incorporating the published handbook values of the Young's modulus and the yield stress into the curve. The FEM input curve for beta brass was extrapolated from published values of Young's modulus and yield stress (60). If these input curves themselves reached higher levels than the experimentally predicted curves for these materials, then the FEM calculated curve of alpha-beta brass would reach higher levels than the experimental stress-strain curve. This is because the FEM calculated curve is calculated from the FEM input curves of the alpha and beta brass. The modulus of elasticity of the FEM calculated curve is about 1.04×10^{8} KPa which agrees well with the published handbook value of 1.03×10^{8} KPa (see Table 1). The yield strength value of the FEM and the experimental stress-strain curve is about 170 MPa. This value agrees well with the published handbook values of 150-380 MPa (see Table 1). The grain-size and the phase distribution in the mesh used for the FEM calculation of the stress-strain curve is presented in Figure 5(a).

V. CONCLUSIONS

V-A. TEM Studies

1) The dislocations in polycrystalline specimens deformed to 5 percent strain level, were confined to definite single slip bands. No cross-slip was observed in specimens deformed to this strain level. On the other hand, in specimens that were deformed to 8 percent strain, dislocations moving in intersecting slip planes tangled with each other forming complex dislocation structures.

2) Extensive dislocation pile-ups were observed at the boundary in specimens strained to 5 percent, and as well as the 8 percent strain level. In specimens deformed to 8 percent strain level, dislocations piled-up at the boundary initiated slip in the adjacent grain.

3) "Dislocation-Pairs" were observed in the alpha-phase of the deformed alpha-beta brass. The "Dislocation-Pairs" were observed to occur in pairs near a boundary and not away from it. Burgers vector analysis of such pairs of dislocations indicates that these are SCREW dislocations that may have cross-slipped onto parallel planes and present as pairs in a relaxed configuration under the absence of any applied stress.

V-B. FEM Analysis

1) Stress-strain curves obtained for alpha-beta brass containing 60 volume percent beta phase tends to be higher than the one for 40 volume percent beta phase in the plastic range. The stress-strain curve of alpha-beta brass containing 40 volume percent beta phase is in turn higher than the stress-strain curve for a distribution of 20 volume percent beta phase in the plastic range.

2) For a given volume fraction of beta phase, the FEM calculated stress-strain curves with a finer beta phase distribution tend to be higher than those with a coarser beta phase distribution.

3) Stress distributions both in the loading Y-direction and the transverse X-direction show gradients. Stresses in the beta phase were found to be higher than the stresses in the alpha phase in the loading Y-direction. The stresses in the transverse X-direction were generally compressive. However, below the externally applied stress level of 172 MPa, the stresses in the transverse X-direction in beta phase were tensile, whereas those in alpha were compressive.

4) Strains in the beta phase were found to be higher than the strains in the alpha phase at the externally applied stress levels. The strains in

the beta phase were generally higher near the alpha-beta interface than in the beta grain interior.

5) The FEM calculated stress-strain curve attained higher stress levels, for similar strain levels as compared to an experimentally calculated stress-strain curve. The values of the yield stresses on both the curves are in good agreement. The Young's modulus value of the FEM calculated curve agrees well with the experimentally predicted data.

VI. REFERENCES

1. A. Hingwe and K.N. Subramanian. "On Growth of Two-Phase Bicrystals of Alpha-Beta Brass." J. Crystal Growth, 21, 287, (1974).

2. A. Hingwe and K.N. Subramanian. "Deformation of Duplex Crystals and Two-Phase Bicrystals of Alpha-Beta Brass." J. Mater. Sci., 10, 183, (1975).

3. A. Hingwe. "Duplex-Crystals and Two-Phase Bicrystals of Alpha-Beta Brass -- Growth and Mechanical Properties, Ph.D. Thesis." Michigan State University, (1973).

4. C. Nilsen and K.N. Subramanian. "Deformation of Alpha-Beta Brass with Oriented and Equiaxed Duplex Geometries." phy. stat. sol., 79, 281, (1983).

5. C. Nilsen and K.N. Subramanian. "Role of Strain Rate and Phase Boundary Geometry on Deformation Behavior of Two-Phase Bicrystals of Alpha-Beta Brass." J. Mater. Sci., 19, 768, (1984).

6. C. Nilsen. "Mechanical Properties of Alpha-Beta Brass -- Studies on Model Systems, Ph.D. Thesis." Michigan State University, (1973).

7. A. Kezri-Yazdan and K. N. Subramanian. "Elevated Temperature Deformation Behavior of Alpha-Beta Brass Bicrystals, Part 1 -- Ordered Beta." J. Mater. Sci., (in Press).

8. A. Kezri-Yazdan and K. N. Subramanian. "Elevated Temperature Deformation Behavior of Alpha-Beta Brass Bicrystals, Part 11 -- Disordered Beta." J. Mater. Sci., (in Press).

9. A. Kezri-Yazdan and K. N. Subramanian. "Elevated Temperature Deformation Behavior of Alpha-Beta Brass Bicrystals, Part 111 -- Supporting Studies." J. Mater. Sci., (in Press).

10. S. Karashima. "Electron Microscope Studies of Deformed Alpha Brass, Part I -- General Arrangement of Dislocations." Trans. J.I.M., 2, 134, (1961).

11. S. Karashima. "Dislocation Pairs Observed in Alpha Brass." Trans. J.I.M., 3, 48, (1962).

12. J. Jinoch, S. Ankem, and H. Margolin. "Calculation of Stress-Strain Distribution for an Alpha-Beta Ti-8Mn Alloy." Mat. Sci. Eng., 34, 203, (1978).

13. S. Ankem and H. Margolin. "Finite Element Method Calculations of Stress-Strain Behavior of Alpha-Beta Ti-Mn Alloys: Part I. Stress-Strain Relations." Metall. Trans. A., 13A, 595, (1982).

14. S. Ankem and H. Margolin. "Finite Element Method Calculations of Stress-Strain Behavior of Alpha-Beta Ti-Mn Alloys: Part II. Stress and Strain Distributions." Metall. Trans. A., 13A, 603, (1982).

15. M. Hansen and K. Anderko. Constitution of Binary Alloys. McGraw-Hill, New York, 650, (1958).

16. Metals Handbook. Properties and Selection of Materials, Volume 1, Edition 8, L. Taylor (Ed.), American Society of Metals, Ohio, 1021, (1961).

17. H. Unckel. J. Inst. Metals, 61, 171, (1937), (as cited in reference 6).

18. H. Chao and L. Van Vlack. "Deformation of Oriented MnS Inclusions on Low-Carbon Steel." Trans. Met. Soc. A.I.M.E., 233, 1277, (1965).

19. R.W.K. Honeycombe and W. Boas. Aust. J. Sci. Res., [A], 1, 70, (1948).

20. L.M. Clarebrough and G. Perger. Aust. J. Sci. Res., [A], 3, 72, (1950).

21. L.M. Clarebrough and G. Perger. Aust. J. Sci. Res., 5, 114, (1952), (as cited in reference 6).

22. J. Gurland. "Comparison of Dispersion Hardening in Four Silver-Base Alloys of Equivalent Compositions." Trans. Met. Soc. A.I.M.E., 221, 407, (1961).

23. H. Margolin, P. Farrar, and M. Greenfield. The Science, Technology and Application of Titanium, R. Jaffe and N. Promisel (Eds.). Pergamon Press, New York, 795, (1970).

24. A. Eberhardt, M. Suerey, and B. Baudelet. "Plane Interface Boundary Sliding in Alpha-Beta Brass." Scripta Metall., 9, 1231, (1975).

25. T. Takasugi, O. Izumi, and N. Fat-Halla. "Activated Slip Systems During Yielding of Alpha-Beta Brass Two-Phase Bicrystals." J. Mater. Sci., 13, 2013, (1978).

26. T. Takasugi, O. Izumi, and N. Fat-Halla. "Plastic Deformation and Fracture Behaviors of Alpha-Beta Brass Two-Phase Bicrystals." Acta Metall., 26, 1453, (1978).

27. T. Takasugi, O. Izumi, and N. Fat-Halla. "Dynamic Observation of Fracture Phenomenon in Alpha-Beta Brass Two-Phase Bicrystals". J. Mater. Sci., 13, 2462, (1978).

28. T. Takasugi, O. Izumi, N. Fat-Halla. "Operative Slip Systems in Alpha-Beta Brass Two-Phase Bicrystals at 150K." J. Mater. Sci., 14, 1651, (1979).

29. A. Kezri-Yazdan and K.N. Subramanian. "Role of Phase Boundary Orientation Relative to the Tensile Axis in Deformation of Two-Phase Bicrystals." (To Be Published).

30. N. Fat-Halla, T. Takasugi, and O. Izumi. "On Elastic Incompatibility During the Deformation of Alpha-Beta Brass Two-Phase Bicrystals." J. Mater. Sci., 15, 3071, (1980).

31. H. Kawazoe, T. Takasugi, and O. Izumi. "Fatigue of Alpha-Beta Brass Two-Phase Bicrystals." Acta Metall., 28, 1253, (1980).

32. T. Takasugi and O. Izumi. "Interface Sliding in Alpha-Beta Brass Two-Phase Bicrystals." Acta Metall., 28, 465, (1980).

33. Y. Chuang and H. Margolin. "Beta Brass Stress-Strain Relations." Metallurg. Trans., 4, 1905, (1973).

34. T. Lee and H. Margolin. "Beta Brass Bicrystal and Tricrystal Stress-Strain Behavior." Metallurg. Trans., 8A, 157, (1977).

35. T. Lee and H. Margolin. "Effective Young's Modulus in Isoaxial Bicrystals and Tricrystals of Beta Brass." Scripta Metall., 11, 713, (1977).

36. H. Margolin, F. Hazareh, and H. Yaguchi. "Grain Boundary Contribution to the Bauschinger Effect." Scripta Metall., 12, 1141, (1978).

37. H. Yaguchi and H. Margolin. "Grain Boundary Contribution to the Bauschinger Effect in Beta Brass Bicrystals." Scripta Metall., 14, 627, (1980).

38. H. Yaguchi and H. Margolin. "Uniaxial Tension and Compression and Cyclic Stress-Strain Behavior of Beta Brass." Scripta Metall., 14, 631, (1980).

39. G. Ogilvie. J. Inst. Met., (81), 49, (1952-53), (as cited in reference 6).

40. H. Margolin, K. Hashimoto, and H. Yaguchi. "Grain Boundary Nucleation of Slip." Scripta Metall., 15, 181, (1981).

41. A. Cottrell. Dislocations and Plastic Flow in Crystals, Claredon Press, Oxford, 107, (1953).

42. G. Ardley and A. Cottrell. Proc. R. Soc., A219, 328, (1953), (as cieted in refernce 6).

43. I. Fourie. "The Life History of Individual Slip Lines During the Plastic Deformation of Alpha Brass Single Crystals." Acta Metall., 8, 88, (1960).

44. T. Mitchell and P. Thornton. Phil Mag., 10, 315, (1964), (as cited in reference 6).

45. M. Marcinkowski, N. Brown, and R. Fisher. "Dislocations configuration in $AuCu_3$ and AuCu Type Superlattices." Acta Metall., 9, 129, (1961).

46. N. Brown. Phil. Mag., 4, 693, (1959), (as cited in reference 6).

47. A. Greninger. Trans. A.I.M.E., 128, 369, (1938), (as cited in reference 6).

48 A. Head, M. Loretto, and P. Humble. "Identification of Burgers Vector and Unstable Directions of Dislocations in Beta Brass." phy. stat. sol., 20, 521, (1967).

49. P. Humble. "A comparison of Electron Microscope Images in Dislocations based on Isotropic and Anisotropic Elasticity Theory." phy. stat. sol., 21, 733, (1967).

50. A. Head. "Unstable Dislocations in Anisotropic Crystals." phy. stat. sol., 19, 185, (1967).

51. R. Dewitt and J. Koehler. Phy. Rew., 116, 1113, (1959), (as cited in reference 50).

52. A. Head, M. Loretto, and P. Humble. "Influence of Large Elastic Anisotropy on the Determination of Burgers Vector of Dislocations in Beta Brass by Electron Microscopy." phy. stat. sol., 20, 505, (1967).

53. O.C. Zienkiewiez. Finite Element Method in Engineering Sciences. McGraw-Hill, New York, (1971).

54. J. Swedlow and R. Smelser. "Discussion on Calculation of Stress-Strain Curve and Stress-Strain Distributions for an Alpha-Beta Ti-8Mn Alloy." Mat. Sci. Eng., 40, 139, (1979).

55. H. Fischmeister, J. Hjalmered, B. Karlsson, G. Lindon, and B. Sundstrom. Third International Conference on Strength of Materials and Alloys. Institute of Metals and Iron and Steel Institute, Cambridge and London, 1, 621, (1973).

56. B. Sundstrom. "Elastic-Plastic Behavior of WC-Co Analyzed by Continuum Mechanics." Mat. Sci. Eng., 12, 265, (1973).

57. B. Karlsson and B. Sundstrom. "Inhomogeneity in Plastic Deformation of Two-Phase Steel." Mat. Sci. Eng., 161, (1974).

58. P. Hirsch, A. Howie, R. Nicholson, D. Pashley, and M. Whelan. Electron Microscopy of Thin Crystals. Butterworths, London, 36, (1965).

59. G. DeSalvo and J. Swanson. ANSYS Engineering Analysis Systems --- Users Manual, 1, Swanson Analysis Systems Inc., Houston, PA.

60. J. H. Westbrook. Mechanical Properties of Intermetalic Compounds. John-Wiley and Sons, 12, (1959).

61. A. Seeger. Dislocations and Mechanical Properties of Crystals. John-Wiley and Sons, New York, 389, (1957).

62. K. N. Subramanian. "Development of Deformation Bands." phy. stat. sol., 74, 683, (1982).